Discretization strategies

Peter Hjort Lauritzen

Atmospheric Modeling and Predictability Section (AMP)
Climate and Global Dynamics Laboratory (CGD)
National Center for Atmospheric Research (NCAR)

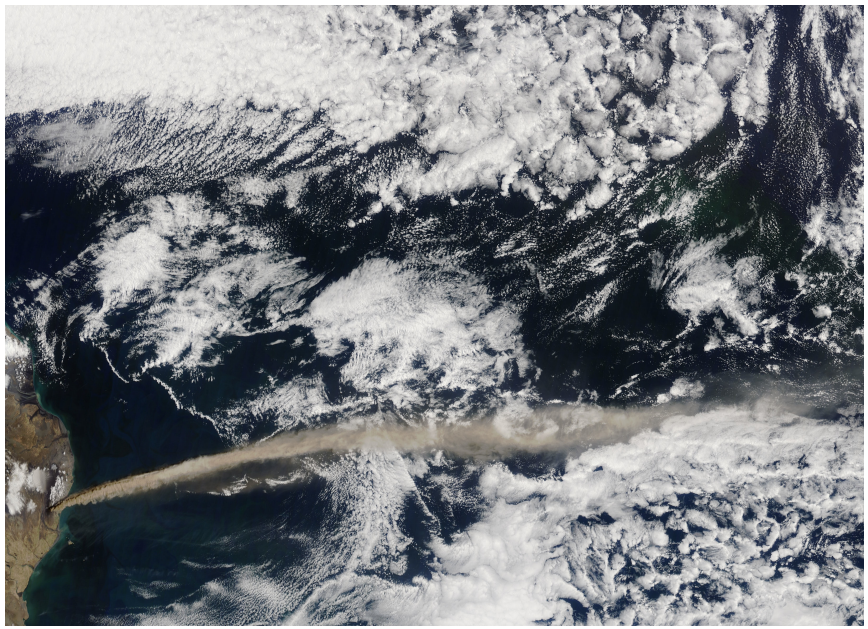

Fundamentals of Atmospheric Chemistry and Aerosol Modeling

Picture: Eruption of Iceland's Eyjafjallajökull volcano (NASA-MODIS)

1. Continuity equation's in climate models

2. Desirable properties for transport schemes intended for climate/climate-chemistry applications
   - Mass-conservation, shape-preservation, multi-tracer efficiency, ...
   - Preservation of pre-existing functional relations (correlations) between species

3. A semi-Lagrangian view on finite-volume schemes

Continuity equations in climate models: dry air

Continuity equation for dry air mass

$$\frac{\partial \rho_d}{\partial t} + \nabla \cdot (\rho_d \vec{v}) = 0,$$

where $\vec{v}$ is the velocity field and ρ_d density.

- Mass of dry air $\approx N_2$ (ca. 78.08%), O_2 (ca. 20.95%), Ar (ca. 0.93%), CO_2 (at present ca. 0.038%); these well-mixed gases make up 99.998% of the volume of dry air
- Trenberth and Smith (2005) estimated that the mass of dry air corresponds to a surface pressure of 983.05 hPa and it varies less than 0.01 hPa based on changes in atmospheric composition.
- $\Rightarrow$ to a very good approximation there are no source/sink terms on the right-hand side of continuity equation for dry air.

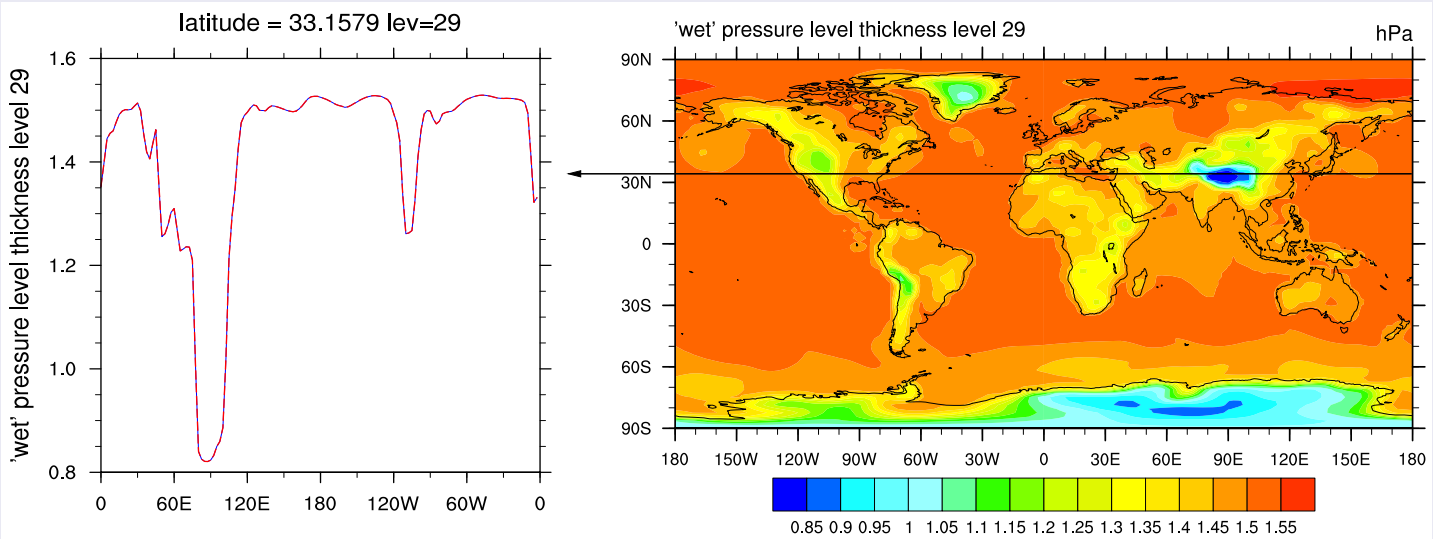

Continuity equations in climate models: water

Continuity equations for water species

$$\frac{\partial (\rho_d m_i)}{\partial t} + \nabla \cdot (\rho_d m_i \vec{v}) = P_{\rho_d m_i},$$

where m_i are dry mixing ratios[a] and P represent source and sink terms.

- m_i: water vapor, cloud liquid and cloud ice.
  - 99% of the total weight of the atmosphere is the mass of dry air. The remanding 1% is approximately the mass of water (large local variations though!)
- m_i: Meso-scale models also have prognostic rain, snow, graupel, ...
  - If rain, snow, graupel, etc. are diagnostic it is assumed that they fall to the ground in one physics time-step!

[a] the subtleties between using 'dry' and 'wet' mixing ratios is not discussed here - see, e.g., Lauritzen et al. (2011b)

Continuity equations in climate models: water

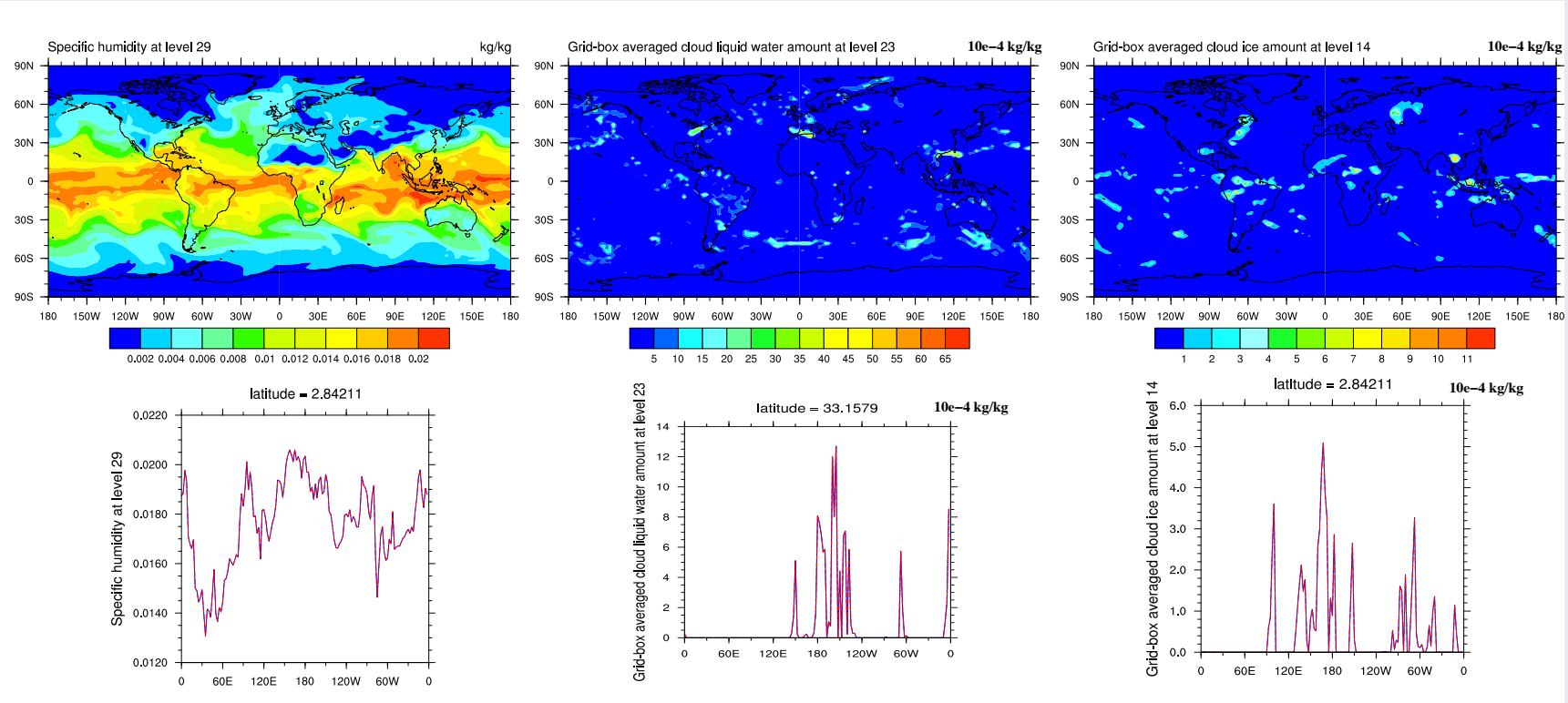

Very 'oscillatory' fields:

- Production/loss terms are large, however, clouds (e.g., 'ice clouds' such as Cirrus) can have lifetimes on the order of days
- Transport operator must not produce negative values.
- Overshooting in water vapor, for example, can trigger irreversible physical processes.

In other words: the transport scheme should be **shape-preserving** with respect to q.

Continuity equations in climate models: aerosols

- Microphysics: continuity equations for aerosol number and mass concentrations
  - CAM5 physics: 22 aerosol continuity equations (particulate organic matter, dust, sea salt, secondary organic aerosols, ...)

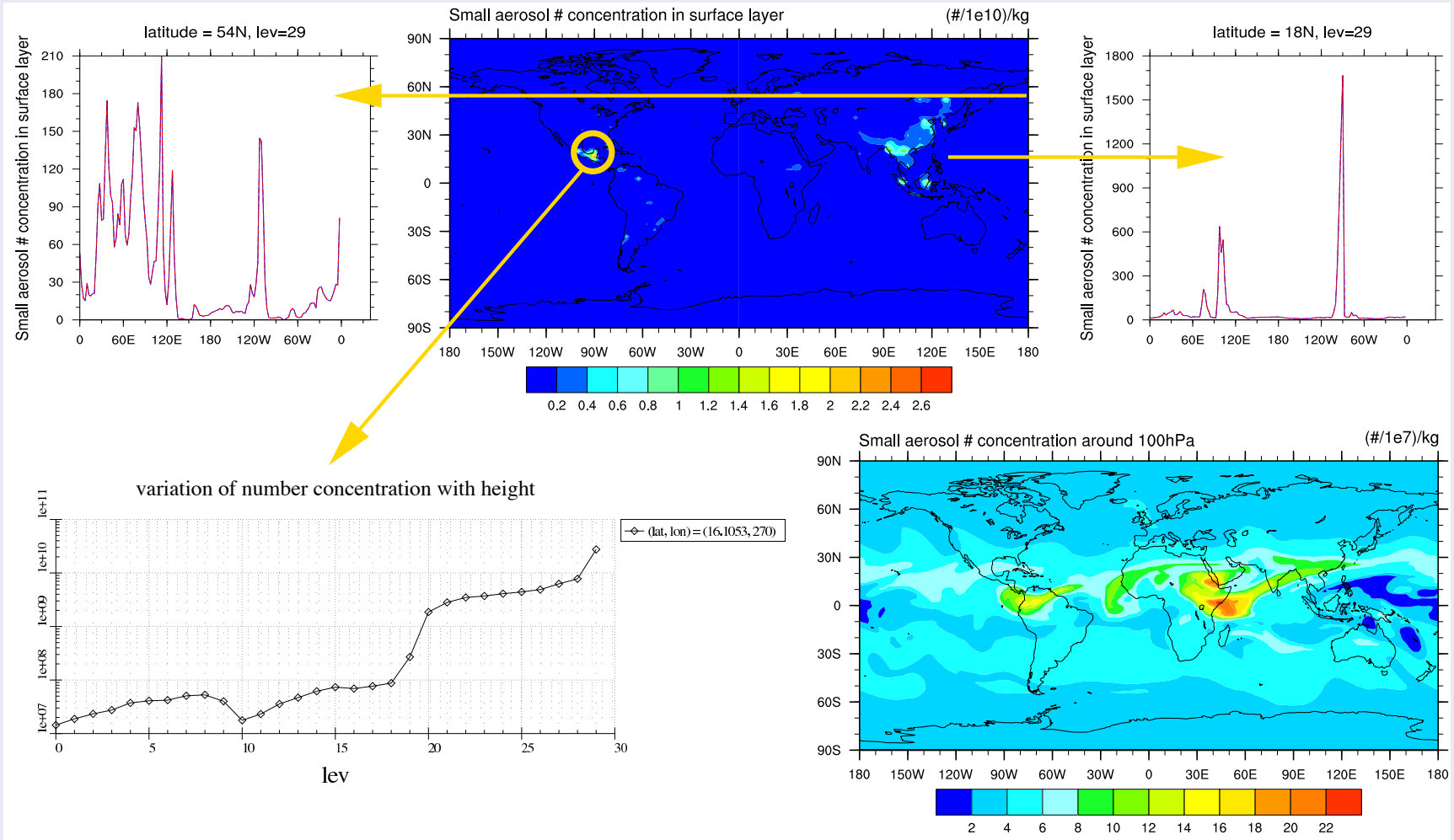

Continuity equations in climate models: chemistry

- Chemistry: continuity equations for chemical species
  - CAM-chem: approximately 127 continuity equations (ozone, chlorine compounds, bromine, ...) ... some highly reactive and some long-lived

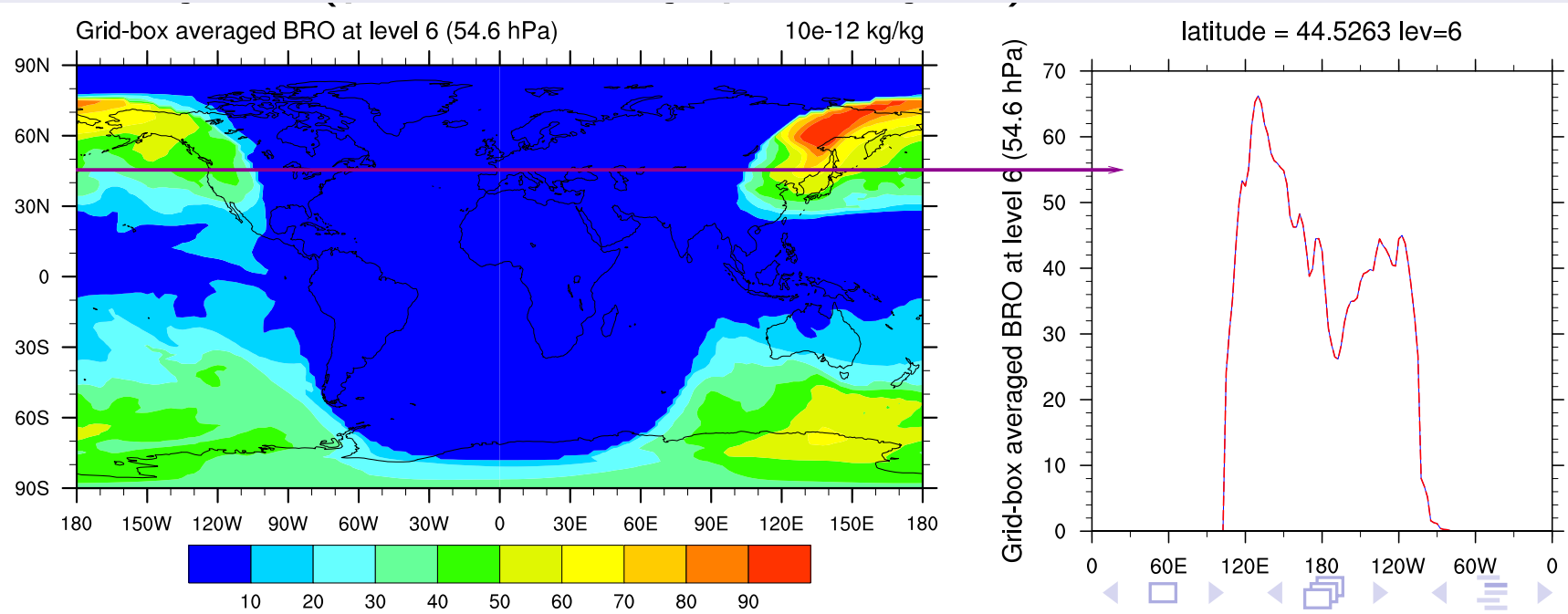

Figure: Bromine has a strong diurnal cycle (produced by photolysis)

Continuity equations in climate models: desirable properties

Important properties of transport schemes intended for atmospheric models:

- The number of prognostic continuity equations in climate and chemistry-climate models is increasing fast to accommodate more advanced physical parameterizations (e.g., microphysics), online chemistry, ...

  $\Rightarrow$ multi-tracer efficiency is becoming increasingly important (closely tied to compute platform)!

- Atmospheric tracer fields can have very large gradients:
  - Shape-preservation is paramount!
  - Preservation of gradients is important
- Inherent conservation of mass is desirable, in particular, to consistently enforce shape-preservation and tracer-air mass consistency.
- Optimal preservation of pre-existing functional relationships (correlations)

Assume a square Cartesian mesh in two dimensions

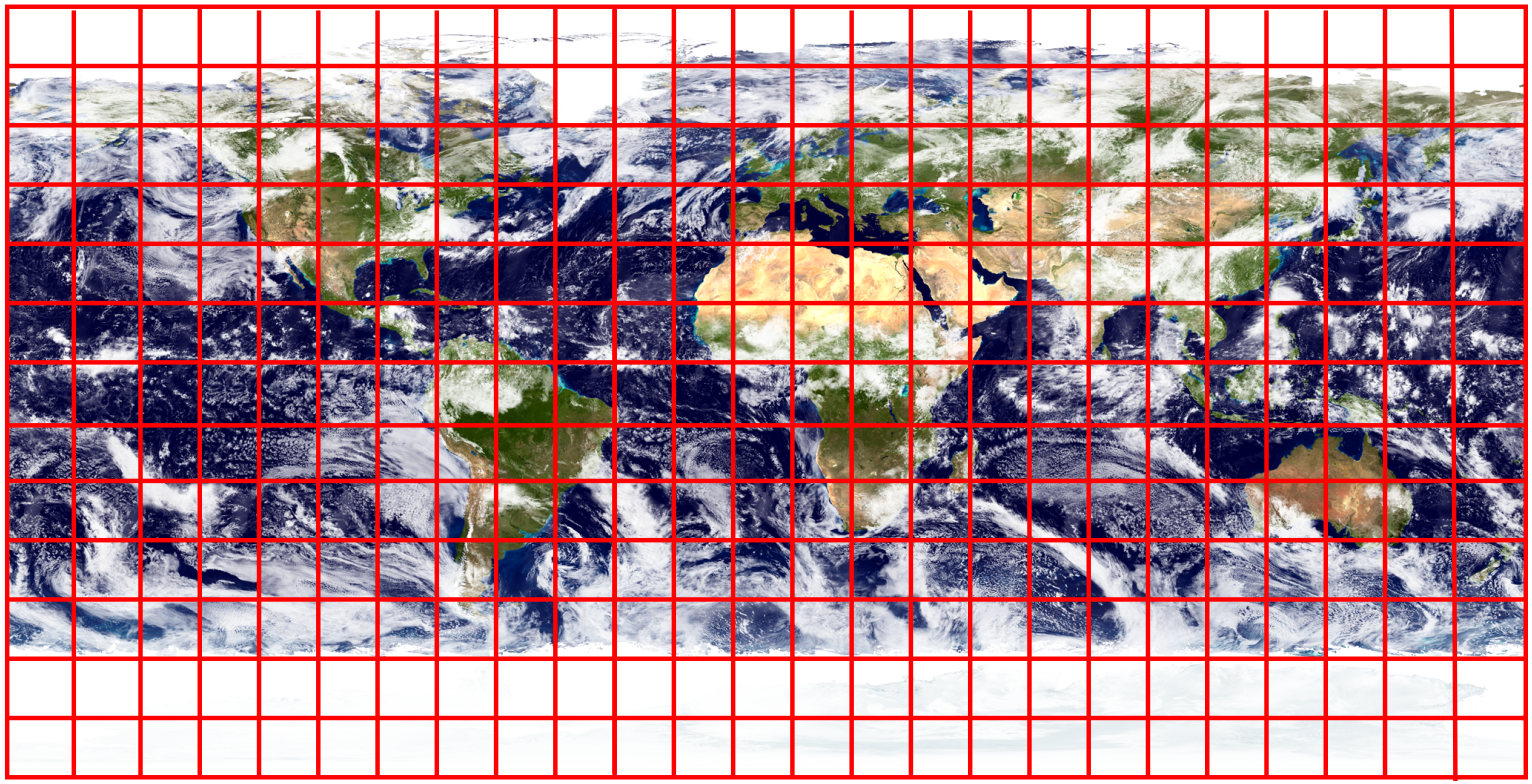

The reformulation of global climate/weather/chemistry models for massively parallel computer architectures + mesh-refinement applications

Traditionally the equations of motion have been discretized on the traditional regular latitude-longitude grid using either

1. spherical harmonics based methods (dominated for over 40 years)
2. finite-difference/finite-volume methods (e.g., CAM-FV)

Both methods require non-local communication:

1. Legendre transform
2. 'polar[a] filters' (due to convergence of the meridians near the poles)

respectively, and are therefore not "trivially" amenable for massively parallel compute systems.

[a] confusing terminology: filters are also applied away from polar regions: $\theta \in [\pm 36^\circ, \pm 90]$

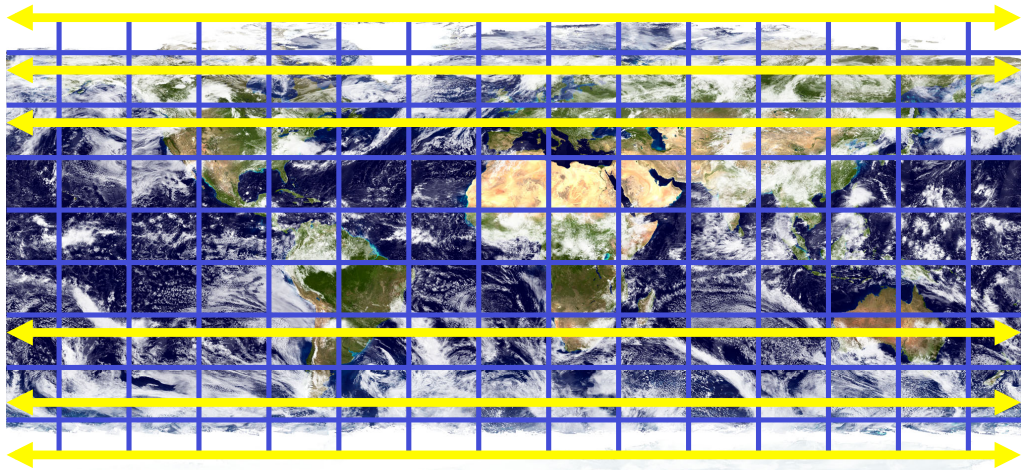

Rectangular computational space

The reformulation of global climate/weather/chemistry models for massively parallel computer architectures + mesh-refinement applications

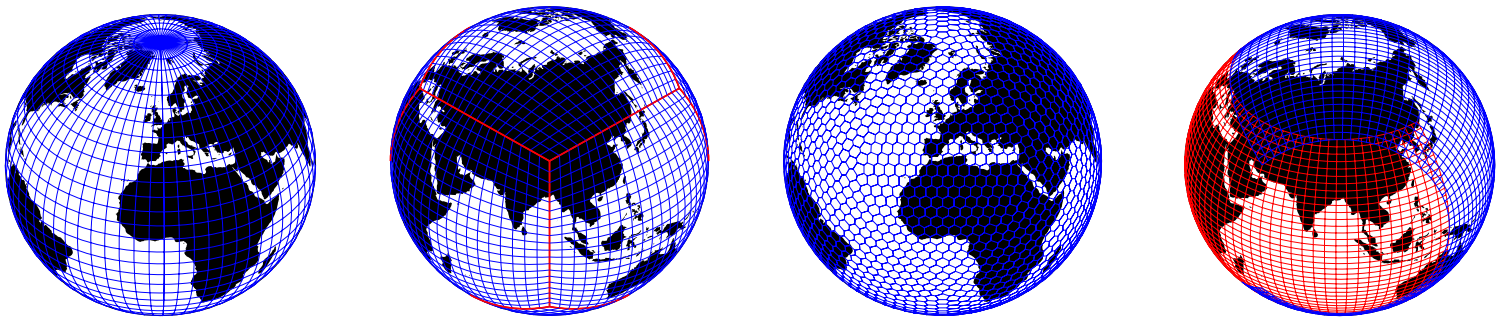

- Quasi-uniform grid + local numerical method ⇒ no non-local communication necessary

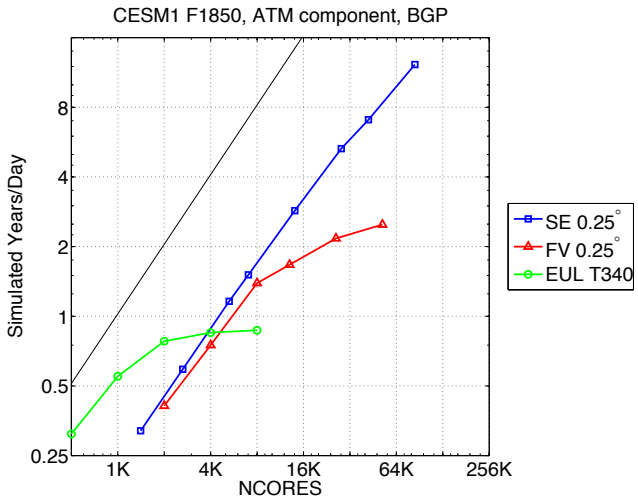

Performance in through-put for different dynamical cores in NCAR's global atmospheric climate model:

horizontal resolution: approximately 25km × 25km grid boxes

- EUL = spectral transform (lat-lon grid)
- FV = finite-volume (reg. lat-lon grid)
- SE = spectral element (cubed-sphere grid)

Computer = Intrepid (IBM Blue Gene/P Solution) at Argonne National Laboratory

Note that for small compute systems CAM-EUL has SUPERIOR throughput!!

The reformulation of global climate/weather/chemistry models for massively parallel computer architectures + mesh-refinement applications

Examples of mesh-refinement. (left) NCAR's Community Atmosphere Model (CAM) based on spectral-elements (SE; Dennis et al., 2012; Lauritzen et al., 2018); (right) NCAR's Model for Prediction Across Scales (MPAS; Skamarock et al., 2012)

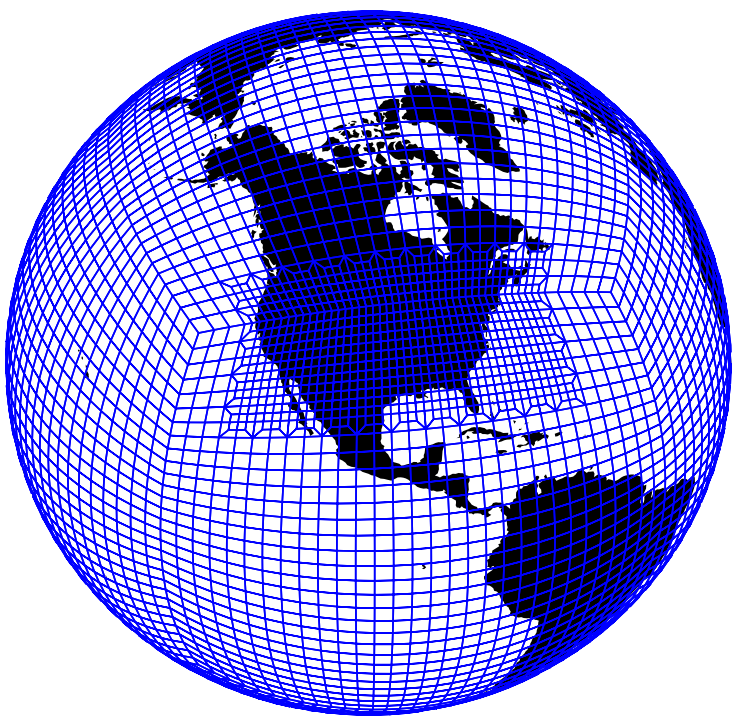

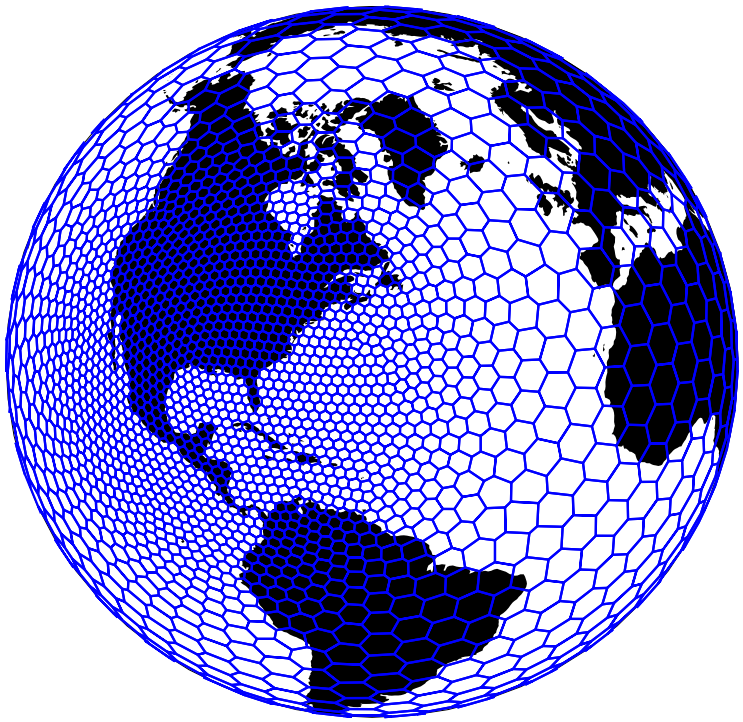

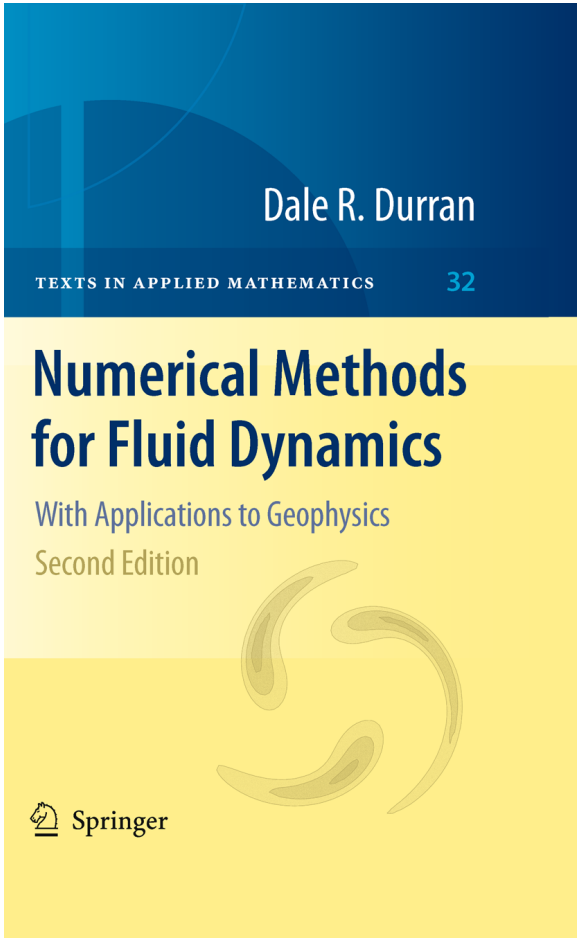

I am going to give a (non-conventional) semi-Lagrangian view on finite-volume discretization schemes!

Derivation form

'Most fundamental equations in fluid dynamics can derived from first principles in either a *Eulerian* form or an *Lagrangian* form' - (see, e.g., text book of Durran, 2010)

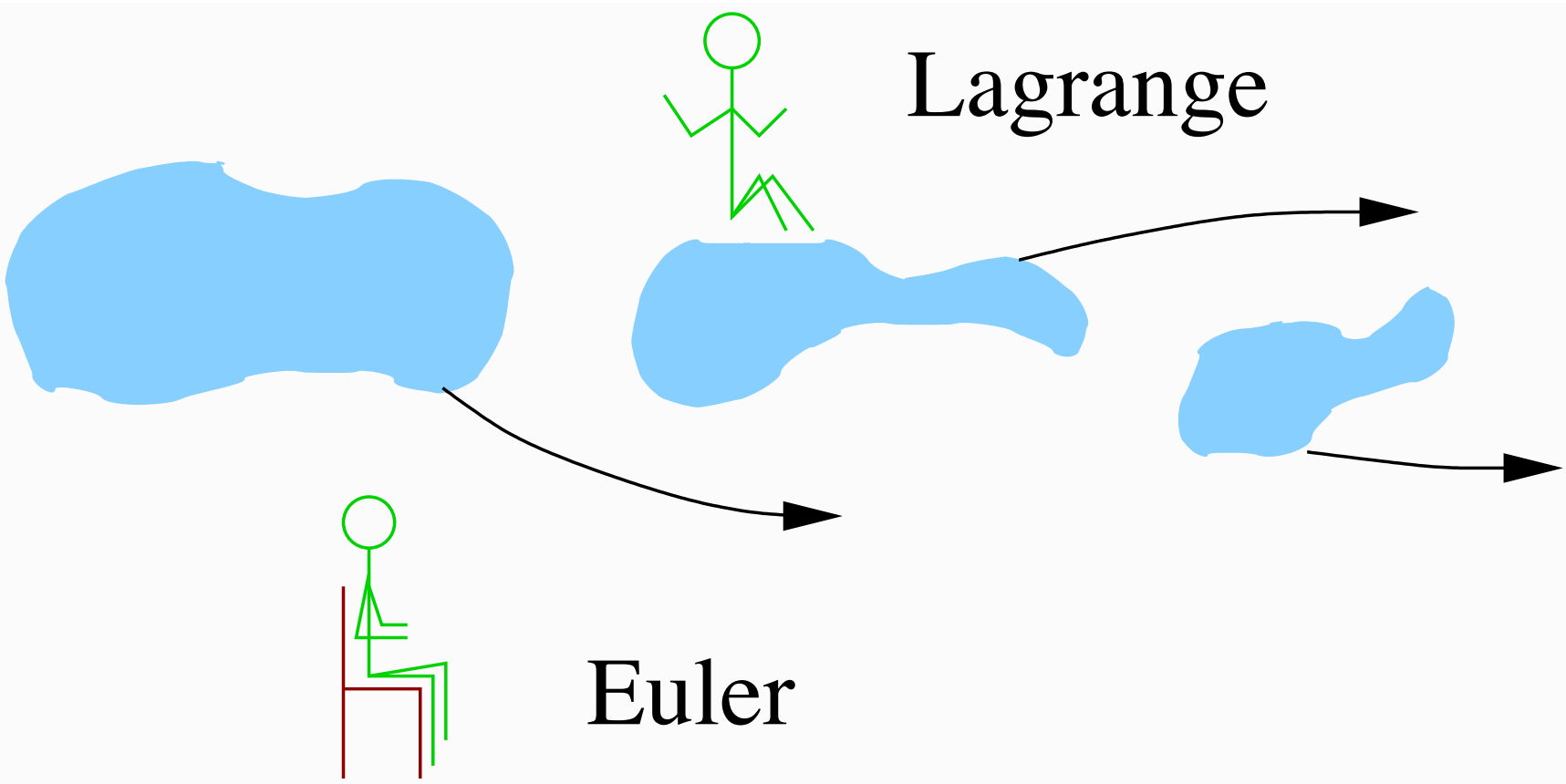

Figure courtesy of J. Thuburn.

Derivation form

Consider the continuity equation for some inert (no sources/sinks) and passive (does not feed back on the flow) tracer

semi-Lagrangian form

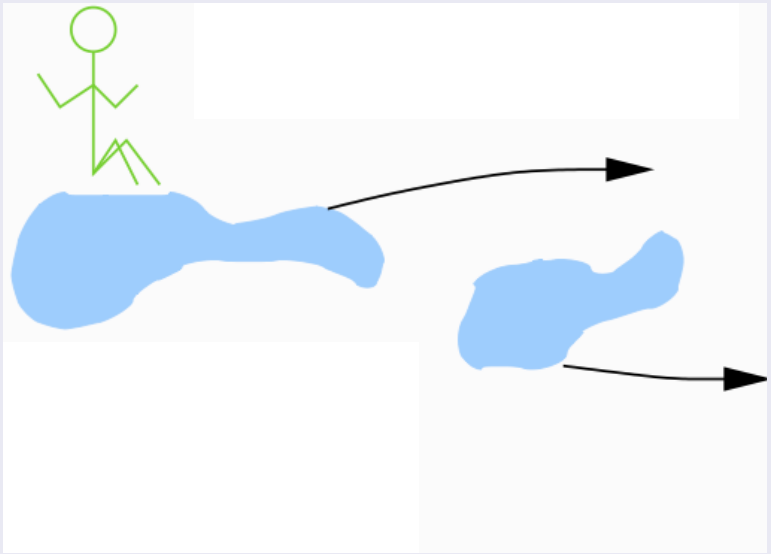

Eulerian (flux) form

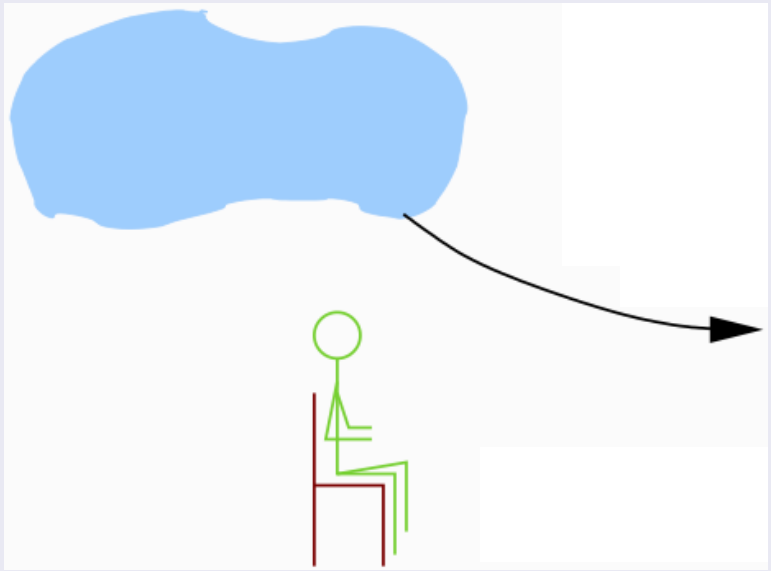

For simplicity assume a quadrilateral mesh (two dimensions) and leave out the 'details' of spherical geometry.

- At first, I'll only consider two-time-level ('area-integrated') finite-volume schemes

Finite-volume approach: Integrate over control volume

semi-Lagrangian form

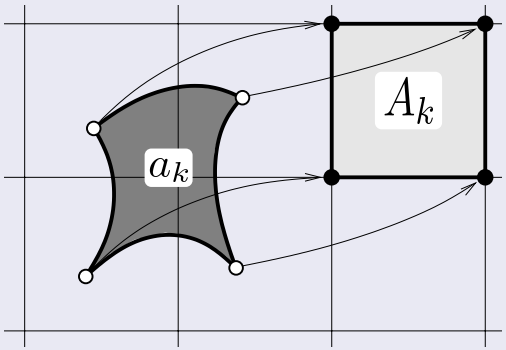

$$\frac{D}{Dt}\int_{A(t)} \psi \, dA = 0.$$

where $A(t)$ is a Lagrangian[†] control volume,

$$\frac{D}{Dt} = \frac{\partial}{\partial t} + \vec{v}\cdot\nabla,$$

is the material/total derivative and $\psi = \rho_d m$.

Eulerian (flux-form) form

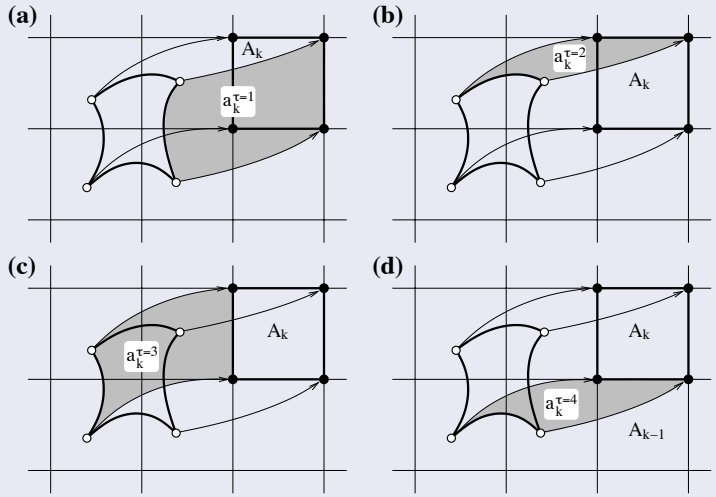

Integrate

$$\frac{\partial \psi}{\partial t} + \nabla\cdot(\psi\,\vec{v}) = 0$$

over an Eulerian control volume A_k:

$$\frac{\partial}{\partial t}\int_{A_k} \psi \, dA + \int_{A_k} \nabla\cdot(\psi\,\vec{v})\, dA = 0.$$

[†] volume whose bounding surface moves with the local fluid velocity $\Leftrightarrow$ volume which always contains the same material particles

Finite-volume approach: Integrate over control volume

semi-Lagrangian form

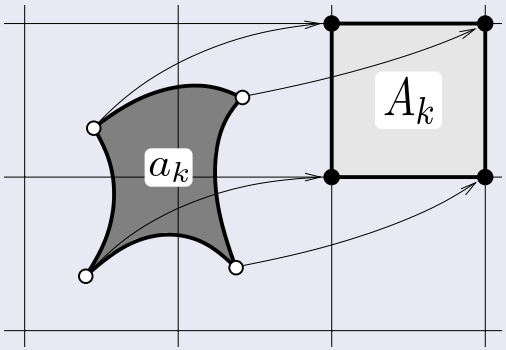

$$\frac{D}{Dt}\int_{A(t)} \psi \, dA = 0.$$

where $A(t)$ is a Lagrangian[†] control volume,

$$\frac{D}{Dt} = \frac{\partial}{\partial t} + \vec{v}\cdot\nabla,$$

is the material/total derivative and $\psi = \rho_d m$.

Eulerian (flux-form) form

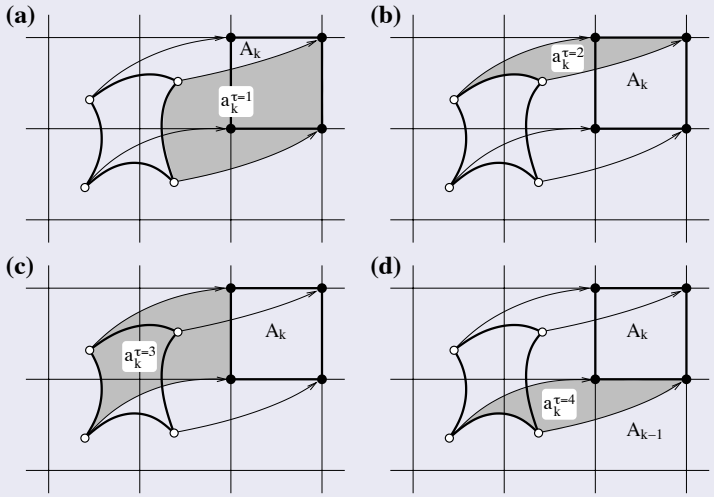

Apply divergence theorem on second term:

$$\frac{\partial}{\partial t}\int_{A_k} \psi \, dA + \oint_{\partial A_k} (\psi \, \vec{v})\cdot\vec{n}\, dS = 0,$$

where ∂A_k is the boundary of A_k and $\vec{n}$ the outward normal vector to ∂A_k.
$\rightarrow$ instantaneous flux of tracer mass through boundaries of A_k

[†] volume whose bounding surface moves with the local fluid velocity $\Leftrightarrow$ volume which always contains the same material particles

Finite-volume approach: Integrate in time

semi-Lagrangian form

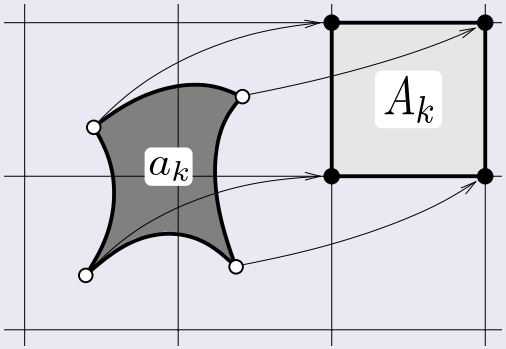

$$\int_{A(t+\Delta t)} \psi \, dA = \int_{A(t)} \psi \, dA,$$

where Δt is time-step and $t = n\,\Delta t$.

Upstream semi-Lagrangian approach:

$$\overline{\psi}_k^{n+1} \Delta A_k = \overline{\psi}_k^n \Delta a_k,$$

where $\overline{()}$ is average value over cell.

Eulerian (flux-form) form

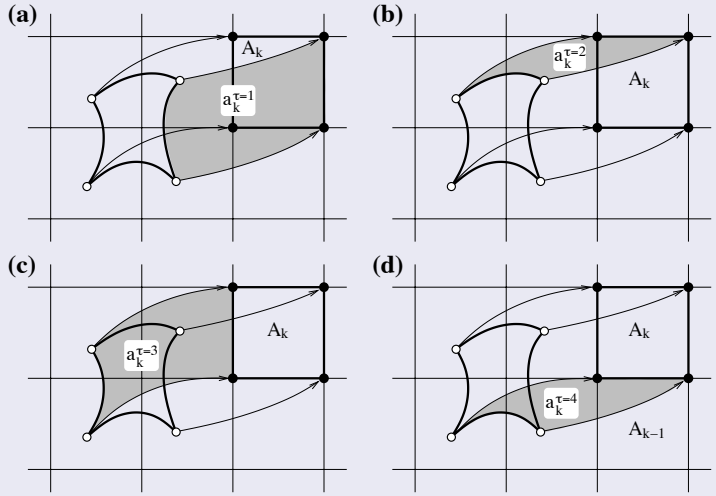

Apply divergence theorem on second term:

$$\frac{\partial}{\partial t} \int_{A_k} \psi \, dA + \oint_{\partial A_k} (\psi \, \vec{v}) \cdot \vec{n} \, dS = 0,$$

where ∂A_k is the boundary of A_k and $\vec{n}$ the outward normal vector to ∂A_k.
$\rightarrow$ instantaneous flux of tracer mass through boundaries of A_k

Finite-volume approach: Integrate in time

semi-Lagrangian form

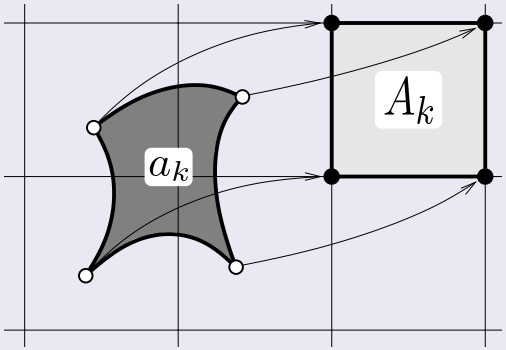

$$\int_{A(t+\Delta t)} \psi \, dA = \int_{A(t)} \psi \, dA,$$

where Δt is time-step and $t = n\,\Delta t$.

Upstream semi-Lagrangian approach:

$$\overline{\psi}_k^{n+1} \Delta A_k = \overline{\psi}_k^n \Delta a_k,$$

where $\overline{()}$ is average value over cell.

Eulerian (flux-form) form

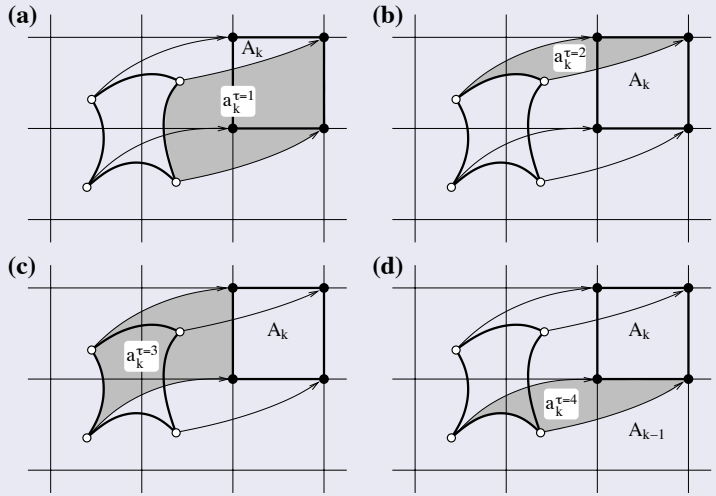

$$\frac{\partial}{\partial t} \int_{A_k} \psi \, dA + \oint_{\partial A_k} (\psi \, \vec{v}) \cdot \vec{n} \, dS = 0,$$

$$\overline{\psi}^{n+1} \Delta A_k = \overline{\psi}^n \Delta A_k +$$

$$\int_{n\Delta t}^{(n+1)\Delta t} \left[\oint_{\partial A_k} (\psi \, \vec{v}) \cdot \vec{n} \, dS \right] dt = 0,$$

$\rightarrow$ flux of tracer mass through boundaries of A_k during $t \in [n\Delta t, (n+1)\Delta t]$

Finite-volume approach:

semi-Lagrangian form

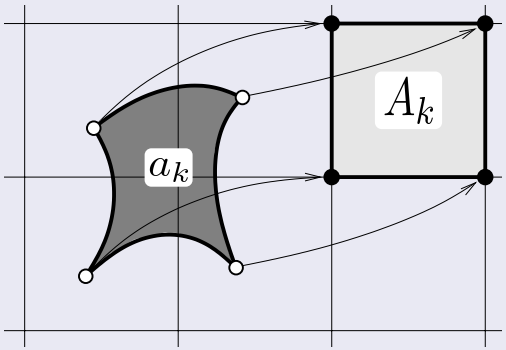

$$\int_{A(t+\Delta t)} \psi \, dA = \int_{A(t)} \psi \, dA,$$

where Δt is time-step and $t = n\,\Delta t$.

Upstream semi-Lagrangian approach:

$$\overline{\psi}_k^{n+1} \Delta A_k = \overline{\psi}_k^n \Delta a_k,$$

where $\overline{()}$ is average value over cell.

Eulerian (flux-form) form

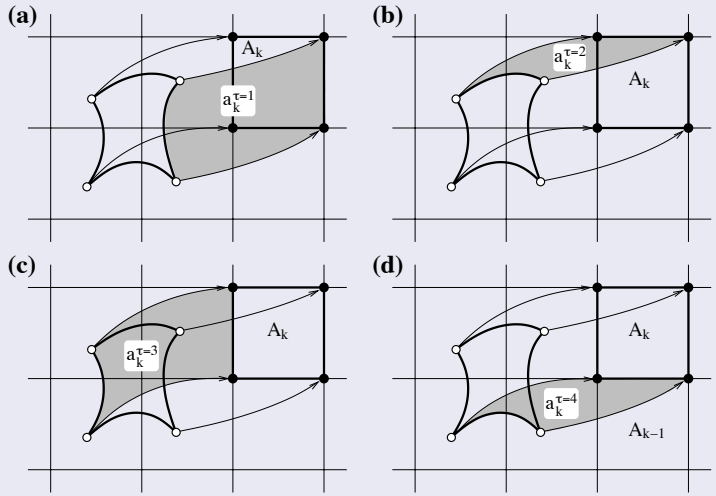

$$\overline{\psi}_k^{n+1} \, \Delta A_k = \overline{\psi}_k^n \, \Delta A_k - \sum_{\tau=1}^{4} F_k^{(\tau)},$$

where

$$F_k^{(\tau)} = s_k^{(\tau)} \int_{a_k^\tau} \psi^n(x,y) \, dA.$$

is flux of mass through face τ during Δt, and $s_k^{(\tau)} = \pm 1$

for simplicity assume s_k^τ is NOT multi-valued; for multi-valued case see, e.g., Harris et al. (2010).

Finite-volume approach:

semi-Lagrangian form

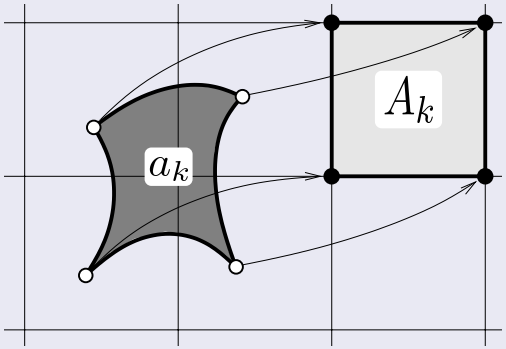

$$\overline{\psi}_k^{n+1} \Delta A_k = \overline{\psi}_k^n \Delta a_k,$$

Eulerian (flux-form) form

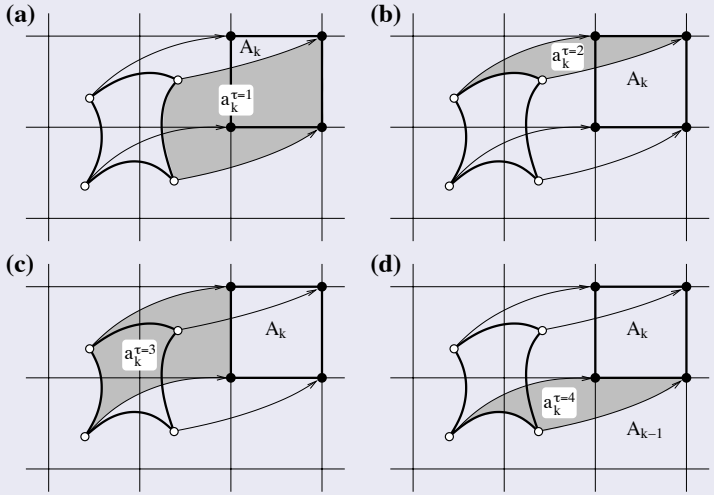

$$\overline{\psi}_k^{n+1} \Delta A_k = \overline{\psi}_k^n \Delta A_k - \sum_{\tau=1}^{4} F_k^{(\tau)},$$

Note equivalence between Lagrangian cell-integrated and Eulerian flux-form continuity equations:

$$\Delta A_k - \sum_{\tau=1}^{4} \left(s_k^{(\tau)} \Delta a_k^{(\tau)} \right) = \Delta a_k.$$

i.e. the areas involved in Eulerian forecast equals upstream Lagrangian area a_k.

Finite-volume approach:

semi-Lagrangian form

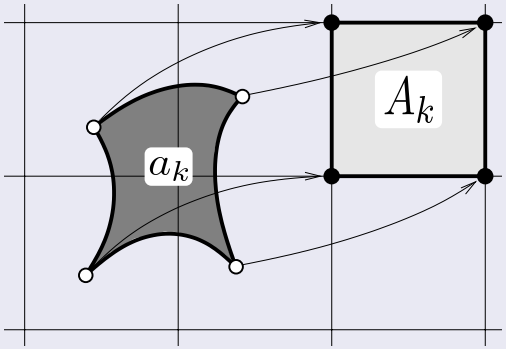

$$\overline{\psi}_k^{n+1} \Delta A_k = \overline{\psi}_k^n \Delta a_k,$$

Define a global piecewise continuous reconstruction function

$$\psi(x,y) = \sum_{k=1}^{N} I_{A_k} \psi_k(x,y),$$

where I_{A_k} is the indicator function

$$I_{A_k} = \begin{cases} 1, \ (x,y) \in A_k, \\ \\ 0, \ (x,y) \notin A_k. \end{cases}$$

Eulerian (flux-form) form

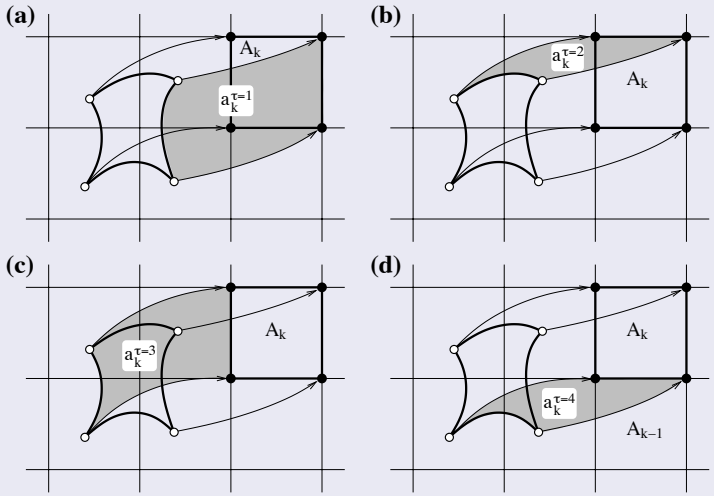

$$\overline{\psi}_k^{n+1} \Delta A_k = \overline{\psi}_k^n \Delta A_k - \sum_{\tau=1}^{4} F_k^{(\tau)},$$

Finite-volume approach:

semi-Lagrangian form

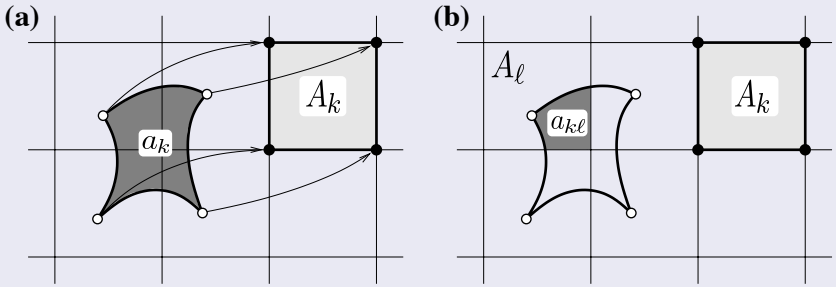

$$\overline{\psi}_k^{n+1} \Delta A_k = \overline{\psi}_k^n \Delta a_k,$$

$$\overline{\psi}_k^{n+1} \Delta A_k = \sum_{\ell=1}^{L_k} \int_{a_{k\ell}} \psi_\ell^n(x,y)\, dA.$$

where $a_{k\ell}$ is the non-empty overlap area

$$a_{k\ell} = a_k \cap A_\ell, \quad a_{k\ell} \neq \emptyset; \quad \ell = 1, \ldots, L_k,$$

where N is the number of cells in the domain and L_k number of overlap areas.

Eulerian (flux-form) form

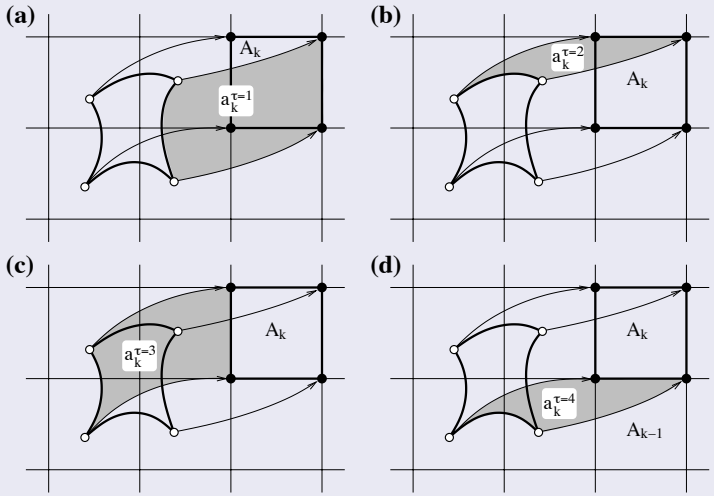

$$\overline{\psi}_k^{n+1} \Delta A_k = \overline{\psi}_k^n \Delta A_k - \sum_{\tau=1}^{4} F_k^{(\tau)},$$

Finite-volume approach:

semi-Lagrangian form

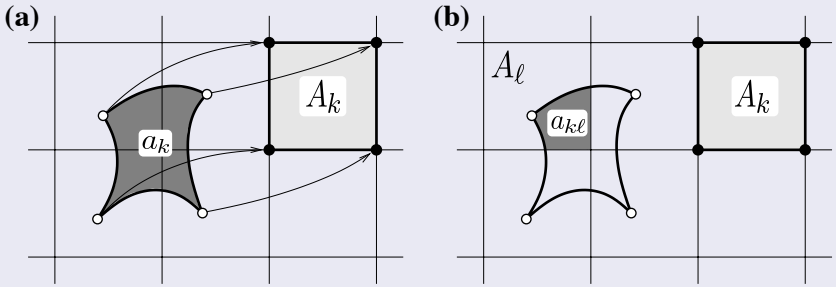

$$\overline{\psi}_k^{n+1} \Delta A_k = \overline{\psi}_k^n \Delta a_k,$$

$$\overline{\psi}_k^{n+1} \Delta A_k = \sum_{\ell=1}^{L_k} \int_{a_{k\ell}} \psi_\ell^n(x,y)\, dA.$$

where $a_{k\ell}$ is the non-empty overlap area

$$a_{k\ell} = a_k \cap A_\ell, \quad a_{k\ell} \neq \emptyset; \quad \ell = 1, \ldots, L_k,$$

where N is the number of cells in the domain and L_k number of overlap areas.

Eulerian (flux-form) form

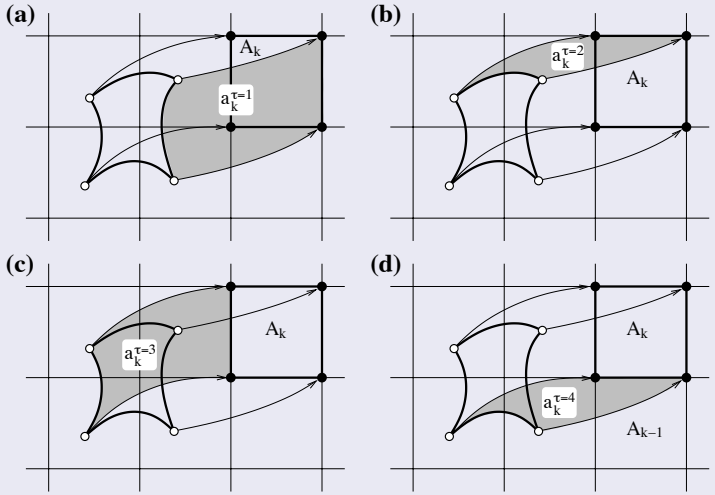

$$\overline{\psi}_k^{n+1} \Delta A_k = \overline{\psi}_k^n \Delta A_k - \sum_{\tau=1}^{4} F_k^{(\tau)},$$

$$F_k^{(\tau)} = \sum_{\ell=1}^{L_k^{(\tau)}} \int_{a_{k\ell}} \psi_\ell^n(x,y)\, dA,$$

where L_k^τ is number of non-empty 'flux' overlap areas for face τ.

Note that in general: $L_k \ll \sum_{\tau=1}^{4} L_k^{(\tau)}$

Finite-volume approach: Conditions for inherent mass-conservation

semi-Lagrangian form

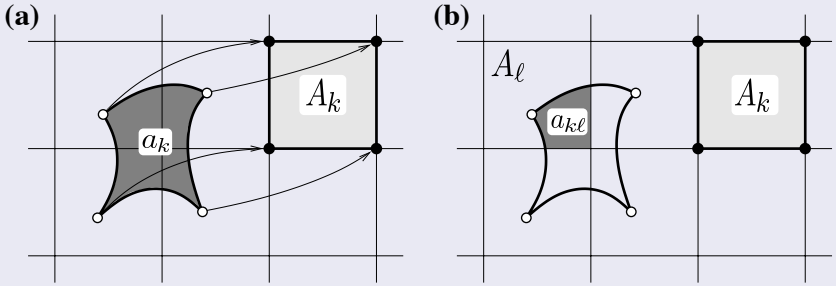

$$\overline{\psi}_k^{n+1} \Delta A_k = \overline{\psi}_k^n \Delta a_k,$$

- a_k's span Ω without gaps/overlaps

$$\bigcup_{k=1}^{N} a_k = \Omega, \text{ and } a_k \cap a_\ell = \emptyset \; \forall \; k \neq \ell.$$

- Sub-grid-scale representation of ψ must integrate to cell-average mass

$$\int_{A_k} \psi_k^n(x, y) \, dA = \overline{\psi}_k^n \Delta A,$$

Eulerian (flux-form) form

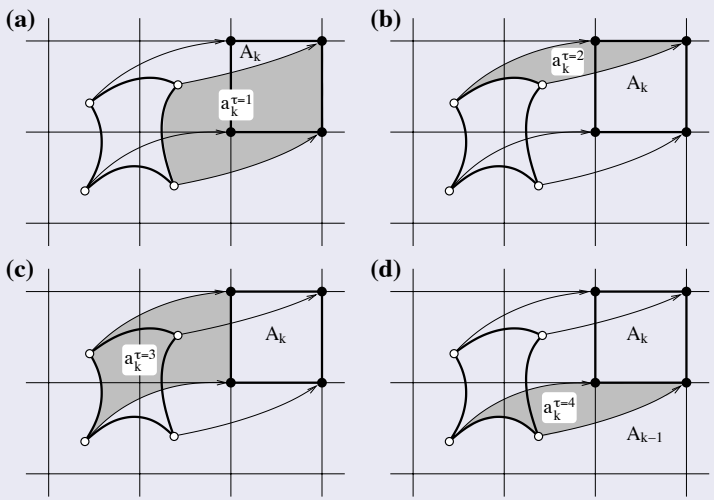

$$\overline{\psi}_k^{n+1} \, \Delta A_k = \overline{\psi}_k^n \, \Delta A_k - \sum_{\tau=1}^{4} F_k^{(\tau)},$$

- Fluxes for 'shared' faces must cancel, e.g.,

$$F_k^{(3)} = -F_{k-1}^{(1)}$$

Any flux, even highly inaccurate fluxes, will NOT violate mass-conservation!

Finite-volume approach: Reconstruction methods for ρ and m

semi-Lagrangian form

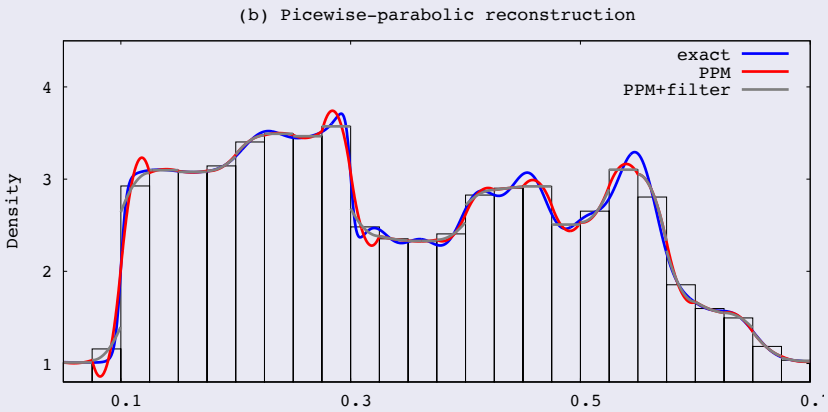

- Inherently mass-conservative PPM (piecewise parabolic method) reconstruction (Colella and Woodward, 1984)
- or variants thereof (PLM, PQM, PSM, ...)

Eulerian (flux-form) form

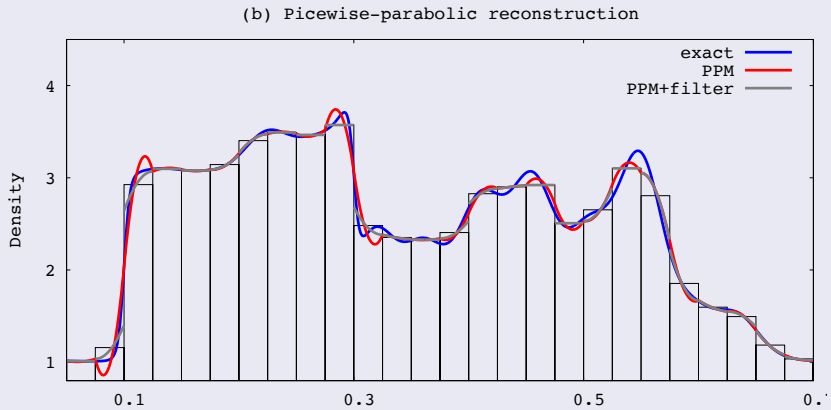

- Inherently mass-conservative PPM (piecewise parabolic method) reconstruction (Colella and Woodward, 1984)
- or variants thereof (PLM, PQM, PSM, ...)
- Any non mass-conservative reconstruction/interpolation method

Note: the higher the order of the polynomial the more extrema (possible over- and under-shoots) $\Rightarrow$ the harder it is to make polynomial shape-preserving (PPM strikes a good balance!)

Finite-volume approach: Enforcing shape-preservation

BAD NEWS!

- (Godunov, 1959): only 1^{st}-order methods are inherently shape-preserving/monotone $\Rightarrow$ higher-order methods need filters for shape-preservation!
- We need to be careful: filter can violate tracer-tracer correlations (e.g., positive definite limiter!
- Also, limiters/filters are inherently non-linear (lots of *if*-statements in the code) $\Rightarrow$ 'bad' for code optimization (e.g., vectorization); limiter can easily be 50% tracer transport cost!
- If your unlimited scheme is 'super duper' accurate (for example, very high order) and you use a 'crappy' limiter $\Rightarrow$ scheme ultimately becomes 'low' order

semi-Lagrangian form

Eulerian (flux-form) form

Finite-volume approach:

semi-Lagrangian form

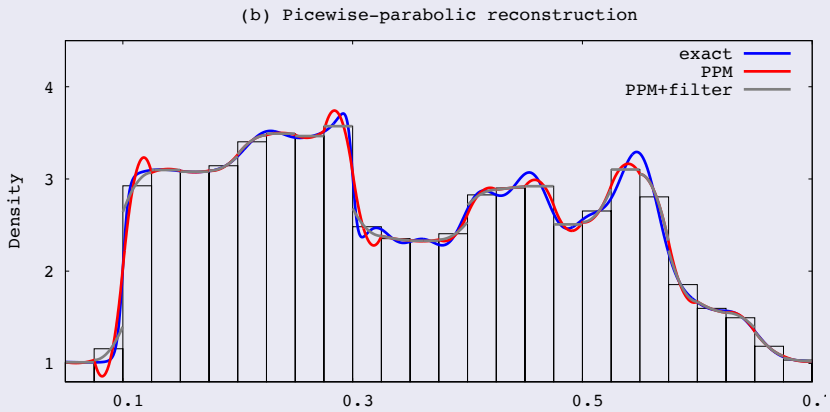

The *only* direct way of enforcing shape-preservation is to filter the sub-grid-scale distribution $\psi_k^n(x, y)$:

- fully 2D filters (Barth and Jespersen, 1989)
- 1D filters for cascade schemes (Colella and Woodward, 1984; Zerroukat et al., 2005; Lin and Rood, 1996)

Eulerian (flux-form) form

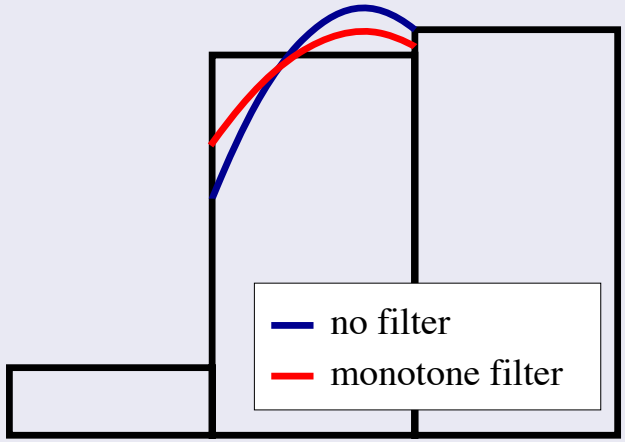

Shape-preservation can be enforced by

- blending monotone and high-order fluxes (e.g., Flux-Corrected Transport Zalesak, 1979)
- 2D filter (Barth and Jespersen, 1989)
- 1D filters for dimensionally split schemes WARNING: may not be shape-preserving for diagonal flow! (Colella and Woodward, 1984; Lin and Rood, 1996)
- WENO-type schemes (selective limiting; Liu et al., 1994)

Finite-volume approach: Area approximation

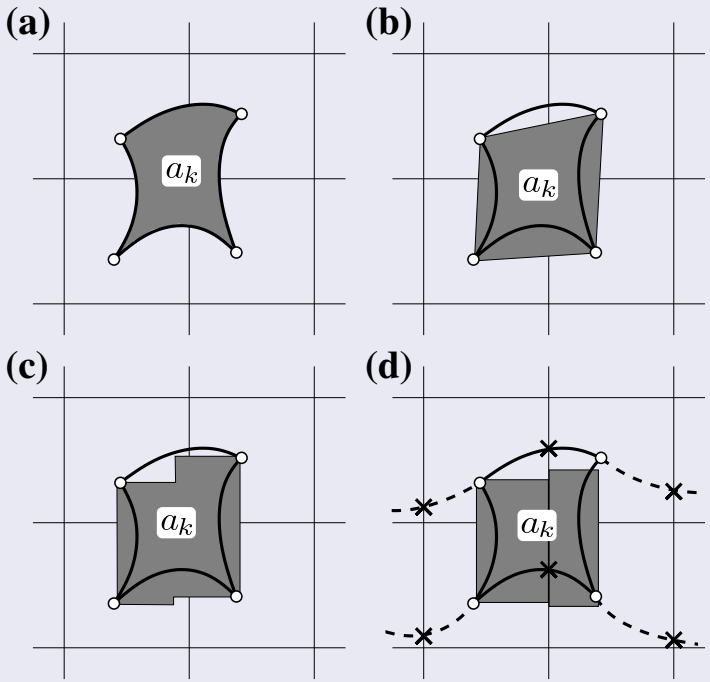

(a) Exact

(b) Straight lines (Rančić, 1992; Lauritzen et al., 2010)

(c) Step-functions for 'North/South' faces & straight lines parallel to 'longitudes' for 'East/West' faces (Nair and Machenhauer, 2002).

(d) Cascade (flow-split) (Nair et al., 2002; Zerroukat et al., 2002)

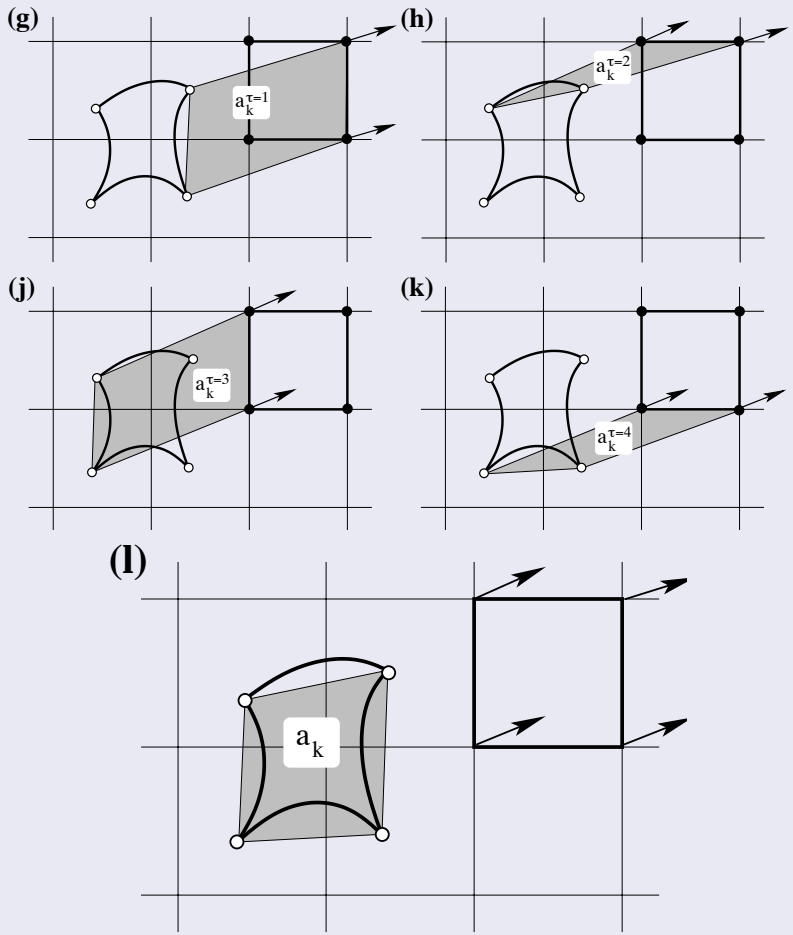

(g-k) Quadrilateral flux-areas (Dukowicz and Baumgardner, 2000; Harris et al., 2010)

(l) 'Effective' departure area

Finite-volume approach: Area approximation

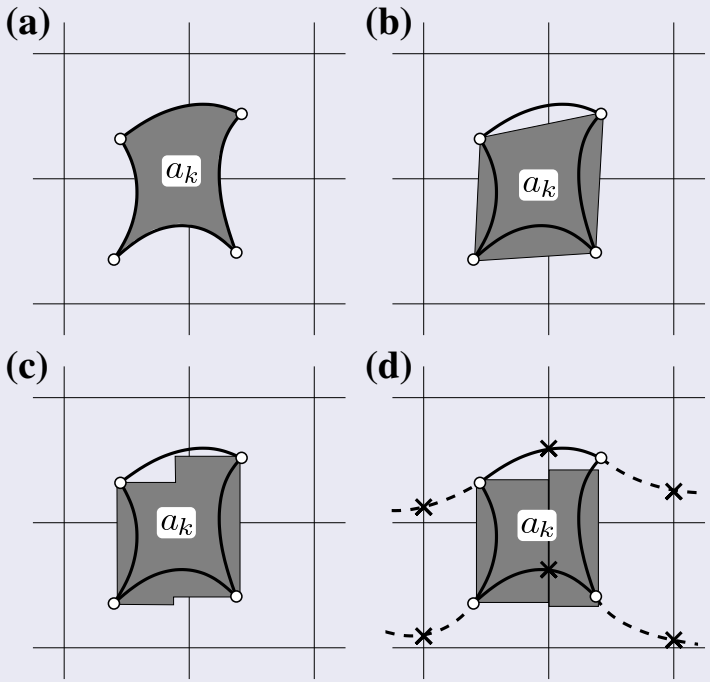

(a) Exact

(b) Straight lines (Rančić, 1992; Lauritzen et al., 2010)

(c) Step-functions for 'North/South' faces & straight lines parallel to 'longitudes' for 'East/West' faces (Nair and Machenhauer, 2002).

(d) Cascade (flow-split) (Nair et al., 2002; Zerroukat et al., 2002)

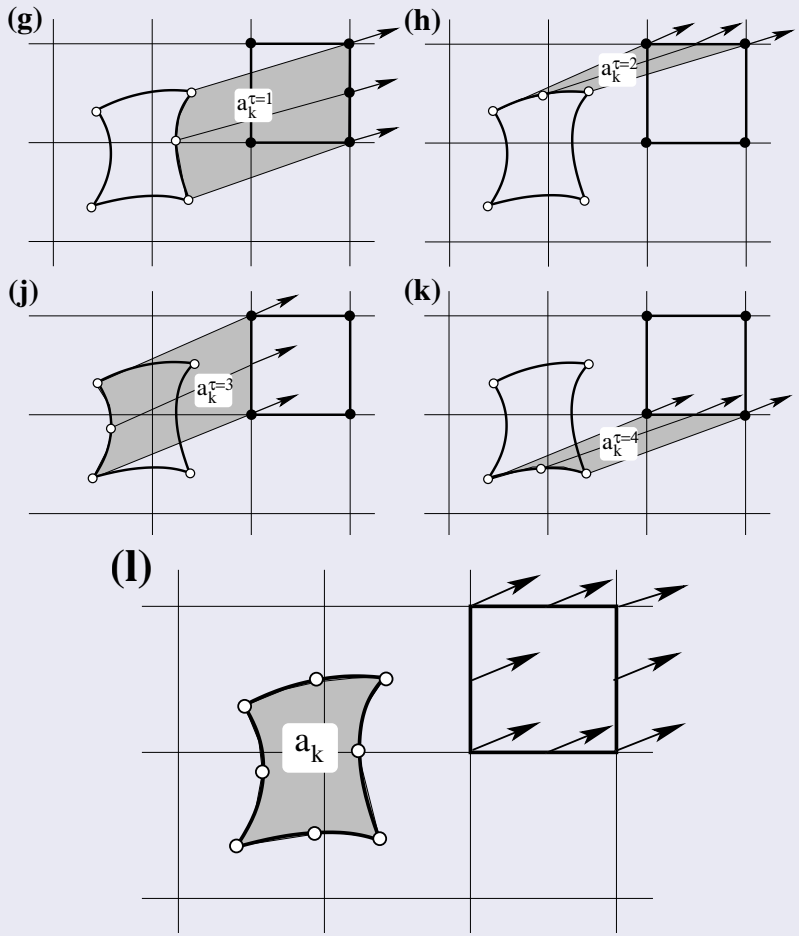

(g-k) 'Curved' (parabolic) flux-areas (Ullrich et al., 2013)

(l) 'Effective' departure area

Finite-volume approach: Area approximation

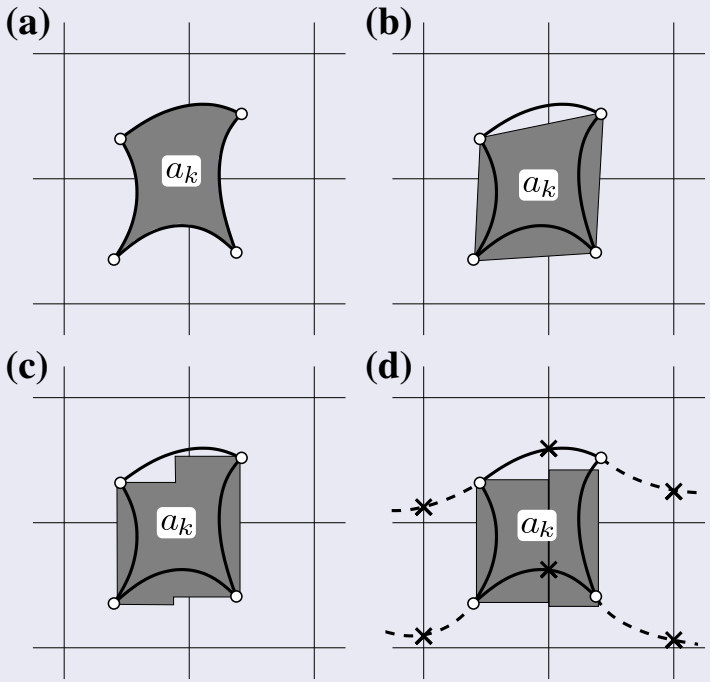

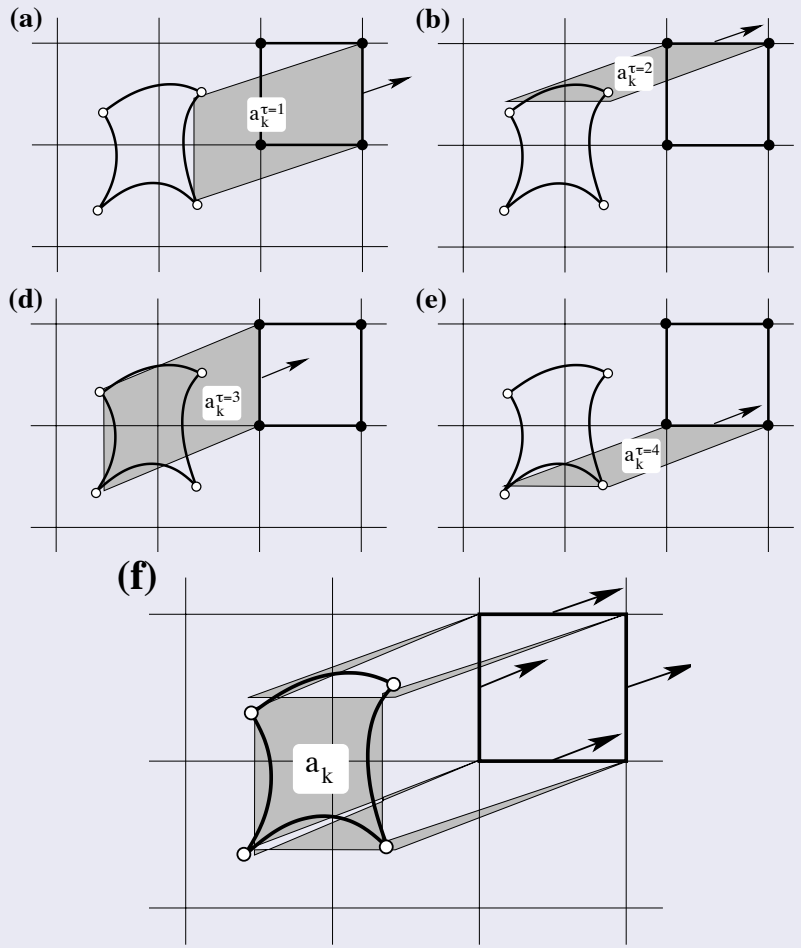

(a) Exact

(b) Straight lines (Rančić, 1992; Lauritzen et al., 2010)

(c) Step-functions for 'North/South' faces & straight lines parallel to 'longitudes' for 'East/West' faces (Nair and Machenhauer, 2002).

(d) Cascade (flow-split) (Nair et al., 2002; Zerroukat et al., 2002)

(g-k) Parallelogram flux-areas (Miura, 2007; Skamarock and Menchaca, 2010)

(l) 'Effective' departure area

Finite-volume approach: Area approximation

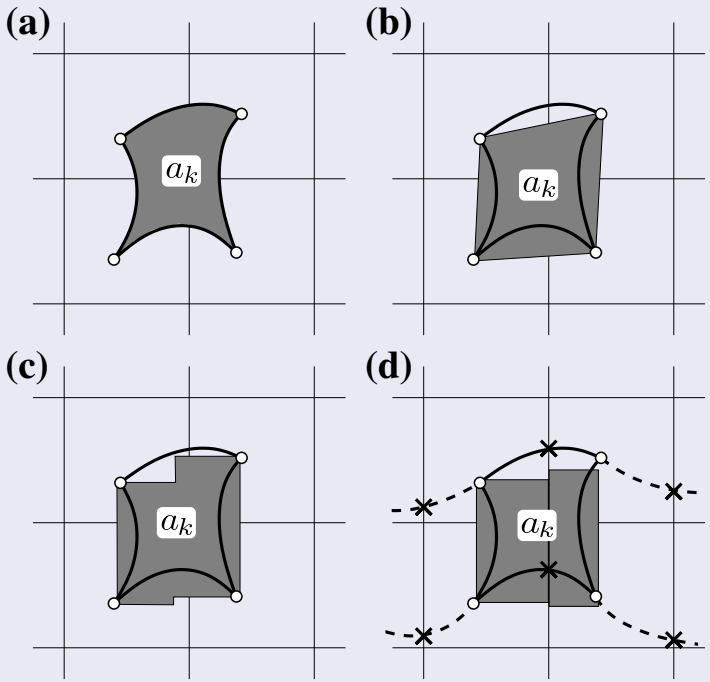

(a) Exact

(b) Straight lines (Rančić, 1992; Lauritzen et al., 2010)

(c) Step-functions for 'North/South' faces & straight lines parallel to 'longitudes' for 'East/West' faces (Nair and Machenhauer, 2002).

(d) Cascade (flow-split) (Nair et al., 2002; Zerroukat et al., 2002)

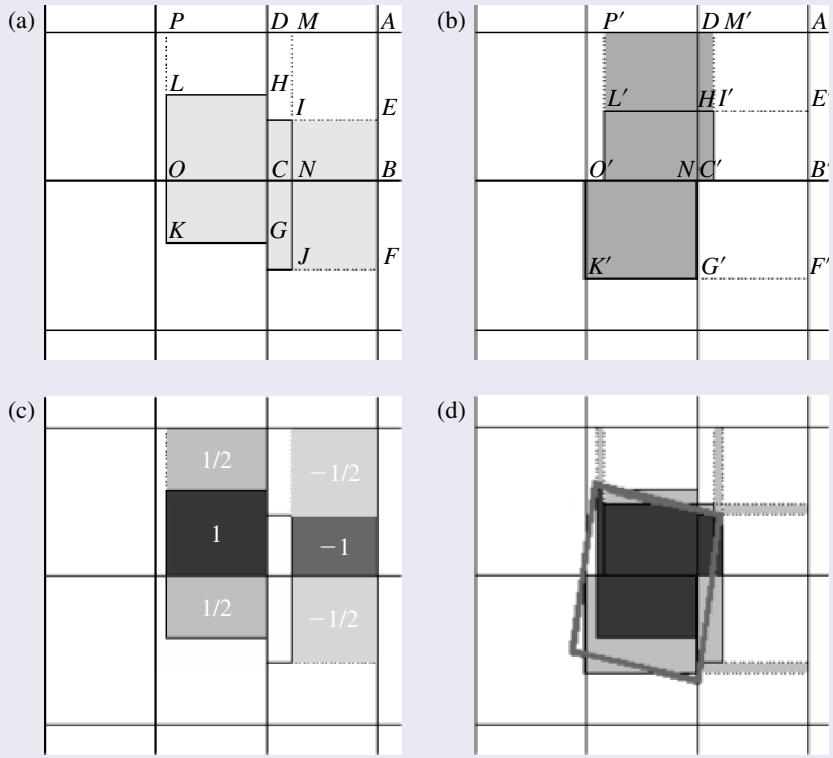

Figure from Machenhauer et al. (2009)

(a-c) Dimensionally split scheme (Lin and Rood, 1996): Flux-areas area combinations of rectangles aligned with grid lines

(d) 'Effective' departure area

Finite-volume approach: Geometric and reconstruction errors

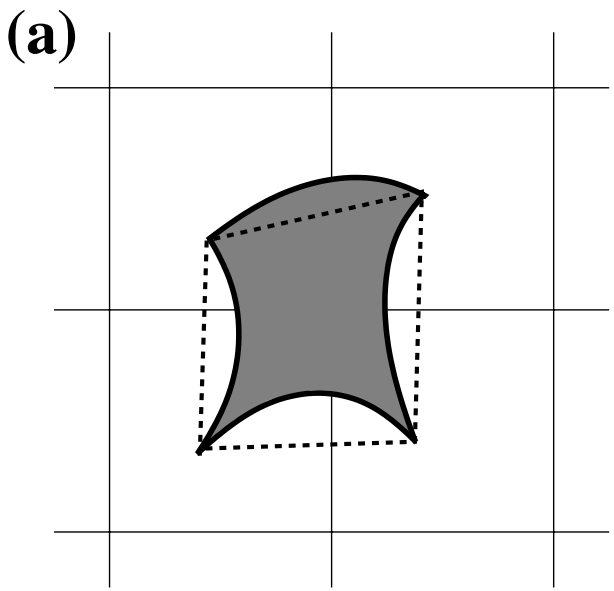

Geometric error

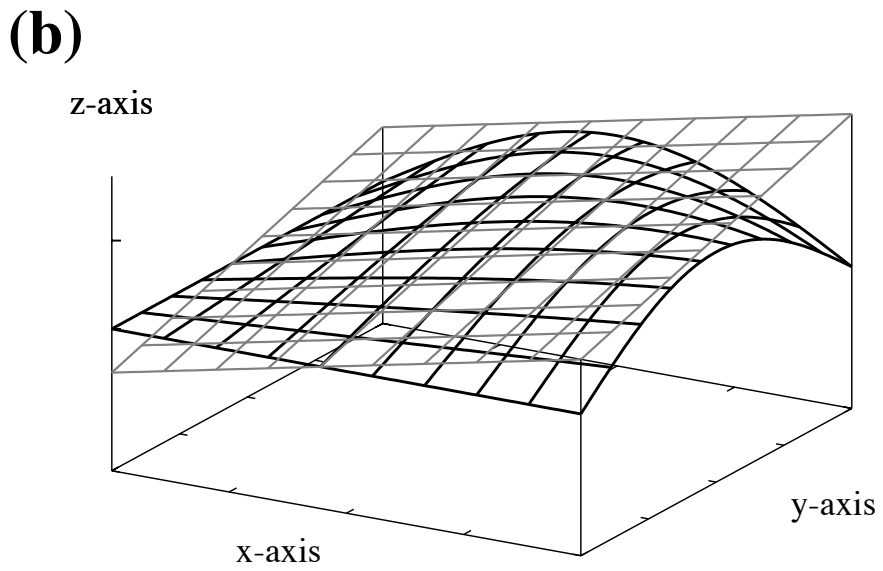

Reconstruction error

- **'geometric error'**: how well is the upstream Lagrangian area / flux areas approximated
- **'reconstruction error'**: how well is the sub-grid-scale distribution approximated

Typically:

- for lower-order reconstruction functions the 'reconstruction error' $\gg$ 'geometric error'
- the smaller the Courant number (Δt) the smaller the 'geometric error'
- for higher-order reconstruction functions and shear flows (deformational) the 'geometric error' can be significant (Ullrich et al., 2013)

Further simplifications for flux-form approaches (Margolin and Shashkov, 2003) - $\frac{u\Delta t}{\Delta x} < 1/2$

Recall: we can do anything we want with the fluxes as long as $F_k^{(3)} = -F_{k-1}^{(1)}$

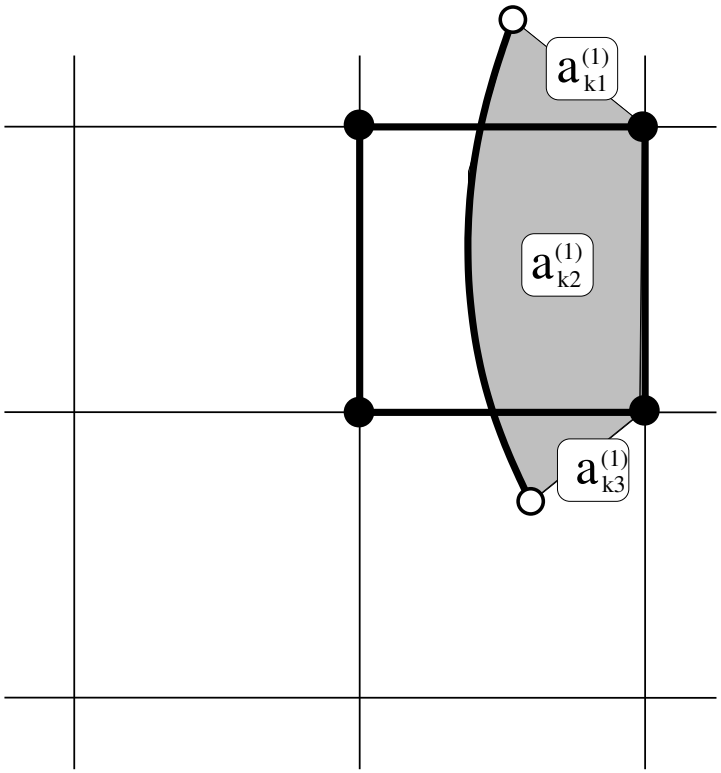

'Rigorous' flux for face 1 ($\tau = 1$):

$$F_k^{(1)} = \sum_{\ell=1}^{3} \int_{a_{k\ell}} \psi_\ell^n(x,y)\, dA.$$

For Δt sufficiently small:

$$\Delta a_{k2} \gg \Delta a_{k1} \text{ and } \Delta a_{k2} \gg \Delta a_{k3}$$

$\rightarrow$ simplify flux-integration by only using one upstream reconstruction function:

$$F_k^{(1)} \approx \mathcal{F}_k^{(1)} = \int_{a_{k1} \cup a_{k2} \cup a_{k3}} \psi_2^n(x,y)\, dA.$$

ψ_2^n **is extrapolated over** a_{k1} **and** a_{k3}**.**

- note: the search for overlap areas has almost been eliminated in $\mathcal{F}_k^{(1)}$
- $\mathcal{F}_k^{(1)}$ stable for Courant numbers approximately less than $\frac{1}{2}$ $(\Delta a_{k2} > \Delta a_{k1} + \Delta a_{k3})$
- $\mathcal{F}_k^{(1)}$ can be slightly more accurate than $F_k^{(1)}$ (Lauritzen et al., 2011a)

MPAS
Model for Prediction Across Scales

Transport - Weighted Sums?

3rd and 4th-order fluxes (e.g. WRF):

$$F(u,\psi)_{i+1/2} = u_{i+1/2}\left[\frac{1}{2}\left(\psi_{i+1}+\psi_i\right) - \frac{1}{12}\left(\delta_x^2\psi_{i+1}+\delta_x^2\psi_i\right) + sign(u)\,\frac{\beta}{12}\left(\delta_x^2\psi_{i+1}-\delta_x^2\psi_i\right)\right]$$

where $\delta_x^2\psi_i = \psi_{i-1} - 2\psi_i + \psi_{i+1}$ *(Hundsdorfer et al, 1995; Van Leer, 1985)*

Recognizing $\delta_x^2\psi = \Delta x^2 \frac{\partial^2\psi}{\partial x^2} + O(\Delta x^4)$ we recast the 3rd and 4th order flux as

$$F(u,\psi)_{i+1/2} = u_{i+1/2}\left[\frac{1}{2}\left(\psi_{i+1}+\psi_i\right) - \Delta x_e^2 \frac{1}{12}\left\{\left(\frac{\partial^2\psi}{\partial x^2}\right)_{i+1} + \left(\frac{\partial^2\psi}{\partial x^2}\right)_i\right\}\right.$$
$$\left. + sign(u)\,\Delta x_e^2 \frac{\beta}{12}\left\{\left(\frac{\partial^2\psi}{\partial x^2}\right)_{i+1} - \left(\frac{\partial^2\psi}{\partial x^2}\right)_i\right\}\right]$$

where *x* is the direction normal to the cell edge and *i* and *i+1* are cell centers. We use the least-squares-fit polynomial to compute the second derivatives.

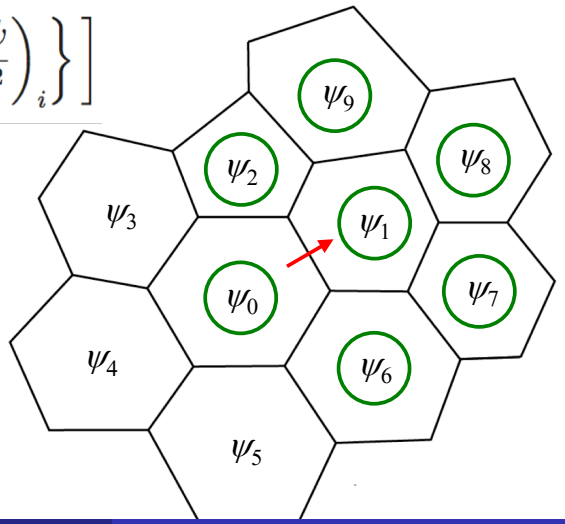

MPAS
Model for Prediction Across Scales

Flux divergence, transport, and Runge-Kutta time integration

Scalar transport equation for cell i:

$$\frac{\partial(\rho\psi)_i}{\partial t} = L(\mathrm{V},\rho,\psi) = -\frac{1}{A_i}\sum_{n_{e_i}} d_{e_i}\left(\rho\mathrm{V}\cdot\vec{n}_{e_i}\right)\overline{\psi}$$

1. Scalar edge-flux value ψ is the weighted sum of cell values from cells that share edge and all their neighbors.
2. An individual edge-flux is used to update the two cells that share the edge.
3. Three edge-flux evaluations and cell updates are needed to complete the Runge-Kutta timestep.
4. Shape-preserving (monotonic) constraint requires checking the cell-value update and renormalizing edge-fluxes if the cell updates are outside specific bounds (on the final RK3 update).

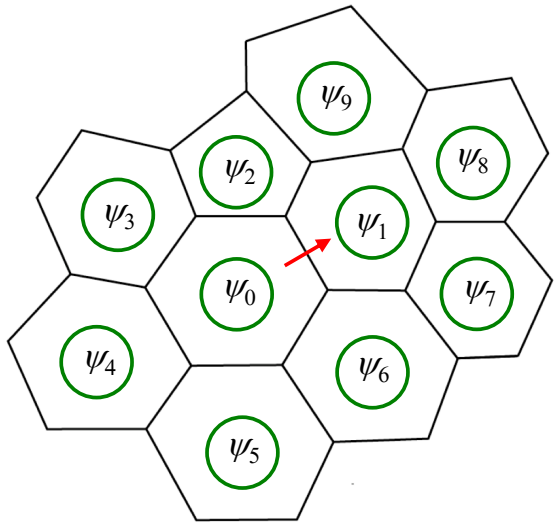

$$(\rho\psi)^* = (\rho\psi)^t + \frac{\Delta t}{3}L(\mathbf{V},\rho,\psi^t)$$

$$(\rho\psi)^{**} = (\rho\psi)^t + \frac{\Delta t}{2}L(\mathbf{V},\rho,\psi^*)$$

$$(\rho\psi)^{t+\Delta t} = (\rho\psi)^t + \Delta t\, L(\mathbf{V},\rho,\psi^{**})$$

Slide from

Time-stepping and coupling: stability

The η-coordinate atmospheric primitive equations, neglecting dissipation and forcing terms:

$$\frac{\partial \vec{v}}{\partial t} + (\zeta + f)\,\hat{k}\times\vec{v} + \nabla\left(\frac{1}{2}\vec{v}^2 + \Phi\right) + \dot{\eta}\frac{\partial \vec{v}}{\partial \eta} + \frac{RT_v}{p}\nabla p = 0 \tag{1}$$

$$\frac{\partial T}{\partial t} + \vec{v}\cdot\nabla T + \dot{\eta}\frac{\partial T}{\partial \eta} - \frac{RT_v}{c_p^* p}\omega = 0 \tag{2}$$

$$\frac{\partial}{\partial t}\left(\frac{\partial p}{\partial \eta}\right) + \nabla\cdot\left(\frac{\partial p}{\partial \eta}\vec{v}\right) + \frac{\partial}{\partial \eta}\left(\dot{\eta}\frac{\partial p}{\partial \eta}\right) = 0 \tag{3}$$

$$\frac{\partial}{\partial t}\left(\frac{\partial p}{\partial \eta}q\right) + \nabla\cdot\left(\frac{\partial p}{\partial \eta}q\vec{v}\right) + \frac{\partial}{\partial \eta}\left(\dot{\eta}\frac{\partial p}{\partial \eta}q\right) = 0. \tag{4}$$

- Continuity equation for air is coupled with momentum and thermodynamic equations:
  - thermodynamic variables and other prognostic variables feed back on the velocity field
  - which, in turn, feeds back on the solution to the continuity equation.
  - Hence the continuity equation for air can not be solved in isolation and one must obey the maximum allowable time-step restrictions imposed by the fastest waves in the system.
- The passive tracer transport equation can be solved in isolation given prescribed winds and air densities, and is therefore not susceptible to the time-step restrictions imposed by the fastest waves in the system.

Time-stepping and coupling: consistency

Continuity equation for air density ρ_d

$$\frac{\partial \rho_d}{\partial t} + \nabla \cdot (\rho_d \, \vec{v}) = 0, \tag{1}$$

and a tracer with mixing ratio q

$$\frac{\partial (\rho_d \, q)}{\partial t} + \nabla \cdot (\rho_d \, q \, \vec{v}) = 0, \tag{2}$$

- In continuous space:

  $q = 1 \Rightarrow$ continuity equation for $(\rho_d \, q)$ reduces to continuity equation for air (ρ_d)

- It is considered desirable that discretization schemes obey this relation:

  'free-stream' preserving or 'consistent' tracer transport.

- Note: 'complete consistency' is obtained if air density and tracer mass continuity equations are solved using the same numerical method, on the same discretization grid, and using the same **time-steps** (everything is 'in sync'!).

Time-stepping and coupling:

semi-Lagrangian form

Eulerian (flux-form) form

Time-stepping and coupling: mass-conservative semi-implicit approach

Traditionally: semi-Lagrangian advection of ρ_d is combined with semi-implicit time-stepping:

$$\overline{\rho_d}_k^{n+1} = \left(\overline{\rho_d}_k^{n+1}\right)_{exp} - \frac{\Delta t}{2}\rho_{d00}\left(\nabla\cdot\vec{v}_k^{n+1} - \nabla\cdot\tilde{\vec{v}}_k^{n+1}\right),$$

where

- ρ_{d00} a constant reference density
- $(\cdot)_{exp}$ is the explicit prediction
- $\tilde{\vec{v}}^{n+1}$ velocity extrapolated to time-level $(n+1)$

What about tracers?

- Solving continuity equation for $(\rho_d\, q)$ explicitly

  $$\overline{\rho_d\, m}_k^{n+1}\Delta A_k = \overline{\rho_d\, m}_k^{n}\Delta a_k$$

  is NOT 'free-stream' preserving!
- Using 'traditional' semi-implicit approach for tracers

  $$\overline{\rho_d\, m}_k^{n+1}\Delta A_k = \overline{\rho_d\, m}_k^{n}\Delta a_k - \frac{\Delta t}{2}(\rho_d\, q)_{00}\left(\nabla\cdot\vec{v}_k^{n+1} - \nabla\cdot\tilde{\vec{v}}_k^{n+1}\right).$$

  is problematic (Lauritzen et al., 2008).

Time-stepping and coupling: mass-conservative semi-implicit approach

Traditionally: semi-Lagrangian advection of ρ_d is combined with semi-implicit time-stepping:

$$\overline{\rho_d}_k^{n+1} = \left(\overline{\rho_d}_k^{n+1}\right)_{exp} - \frac{\Delta t}{2}\left\{\nabla\cdot\left[\left(\overline{\rho_d}_k^{n+1}\right)_{exp}\vec{v}_k^{n+1}\right] - \nabla\cdot\left[\left(\overline{\rho_d}_k^{n}\right)_{exp}\tilde{\vec{v}}_k^{n+1}\right]\right\}.$$

where

- ρ_{d00} a constant reference density
- $(\cdot)_{exp}$ is the explicit prediction
- $\tilde{\vec{v}}^{n+1}$ velocity extrapolated to time-level $(n+1)$

What about tracers?

- A solution is to formulate the semi-implicit terms in flux-form

$$\overline{\rho_d\, m}_k^{n+1} = \left(\overline{\rho_d\, m}_k^{n+1}\right)_{exp} - \frac{\Delta t}{2}\left\{\nabla\cdot\left[\left(\overline{\rho_d\, m}_k^{n+1}\right)_{exp}\vec{v}_k^{n+1}\right] - \nabla\cdot\left[\left(\overline{\rho_d\, m}_k^{n}\right)_{exp}\tilde{\vec{v}}_k^{n+1}\right]\right\}.$$

  so that reference states are eliminated (Wong et al., 2013)

Time-stepping and coupling: Eulerian flux-form

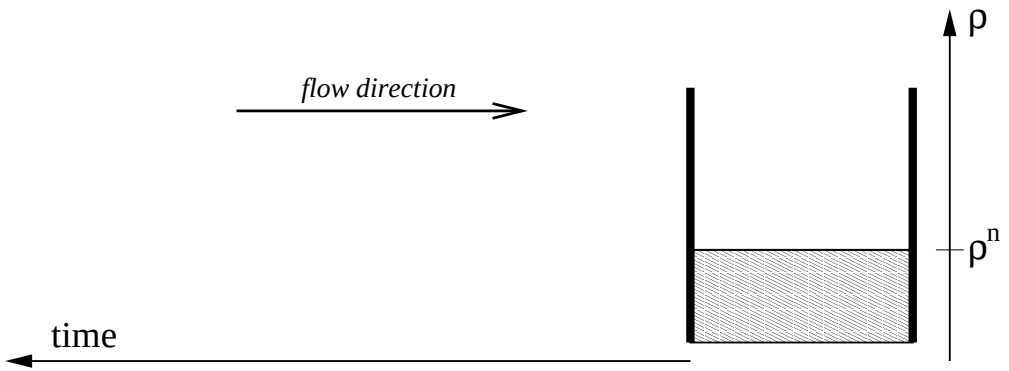

For efficiency, sub-cycle dynamics with respect to tracers:

- Solve continuity equation for air ρ_d together with momentum and thermodynamics equations.
- Repeat *ksplit* times
- Brown area = average flow of mass through cell face.
- Compute time-averaged value of m across brown area using flux-form scheme: $\overline{\overline{< m >}}$.
- Flux of tracer mass: $\overline{\overline{< m >}} \times \sum_{i=1}^{ksplit} {\rho_d}^{n+i/ksplit}$
- Yields 'free stream' preserving solution!

Time-stepping and coupling: Eulerian flux-form

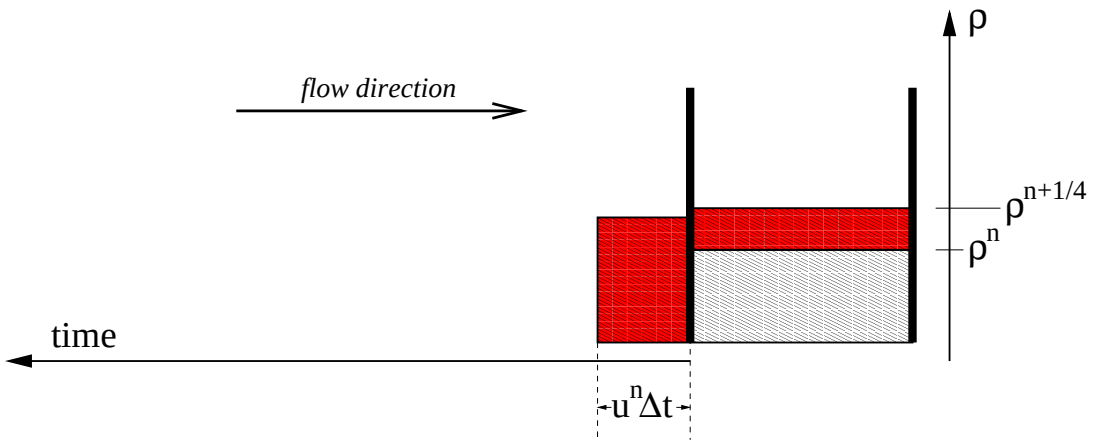

For efficiency, sub-cycle dynamics with respect to tracers:

- Solve continuity equation for air ρ_d together with momentum and thermodynamics equations.
- Repeat *ksplit* times
- Brown area = average flow of mass through cell face.
- Compute time-averaged value of m across brown area using flux-form scheme: $\overline{\overline{< m >}}$.
- Flux of tracer mass: $\overline{\overline{< m >}} \times \sum_{i=1}^{ksplit} {\rho_d}^{n+i/ksplit}$
- Yields 'free stream' preserving solution!

Time-stepping and coupling: Eulerian flux-form

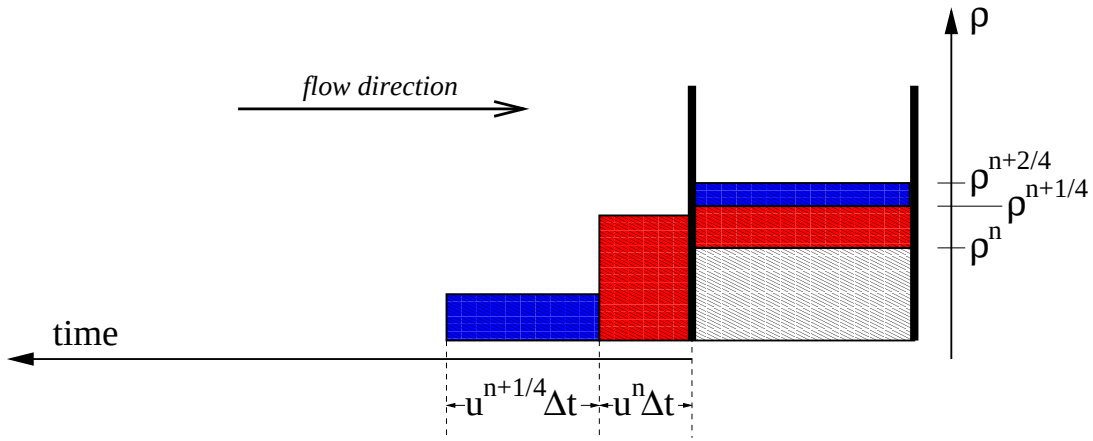

For efficiency, sub-cycle dynamics with respect to tracers:

- Solve continuity equation for air ρ_d together with momentum and thermodynamics equations.
- Repeat *ksplit* times
- Brown area = average flow of mass through cell face.
- Compute time-averaged value of m across brown area using flux-form scheme: $\overline{\overline{< m >}}$.
- Flux of tracer mass: $\overline{\overline{< m >}} \times \sum_{i=1}^{ksplit} {\rho_d}^{n+i/ksplit}$
- Yields 'free stream' preserving solution!

Time-stepping and coupling: Eulerian flux-form

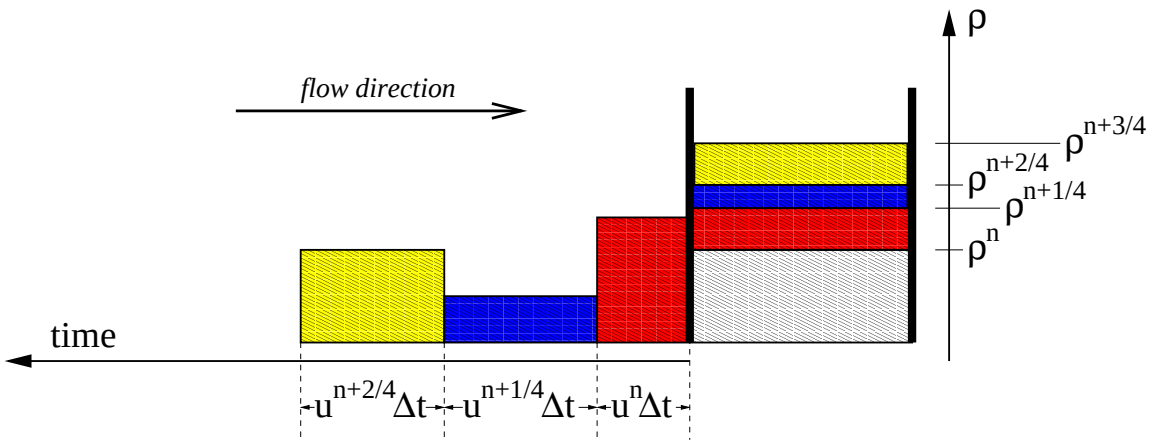

For efficiency, sub-cycle dynamics with respect to tracers:

- Solve continuity equation for air ρ_d together with momentum and thermodynamics equations.
- Repeat *ksplit* times
- Brown area = average flow of mass through cell face.
- Compute time-averaged value of m across brown area using flux-form scheme: $\overline{\overline{< m >}}$.
- Flux of tracer mass: $\overline{\overline{< m >}} \times \sum_{i=1}^{ksplit} {\rho_d}^{n+i/ksplit}$
- Yields 'free stream' preserving solution!

Time-stepping and coupling: Eulerian flux-form

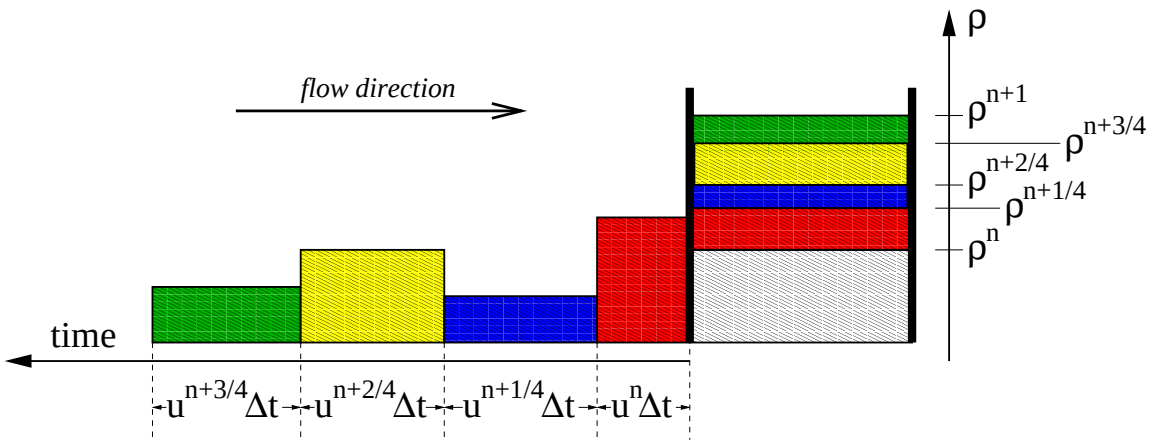

For efficiency, sub-cycle dynamics with respect to tracers:

- Solve continuity equation for air ρ_d together with momentum and thermodynamics equations.
- Repeat *ksplit* times
- Brown area = average flow of mass through cell face.
- Compute time-averaged value of m across brown area using flux-form scheme: $\overline{\overline{< m >}}$.
- Flux of tracer mass: $\overline{\overline{< m >}} \times \sum_{i=1}^{ksplit} {\rho_d}^{n+i/ksplit}$
- Yields 'free stream' preserving solution!

Time-stepping and coupling: Eulerian flux-form

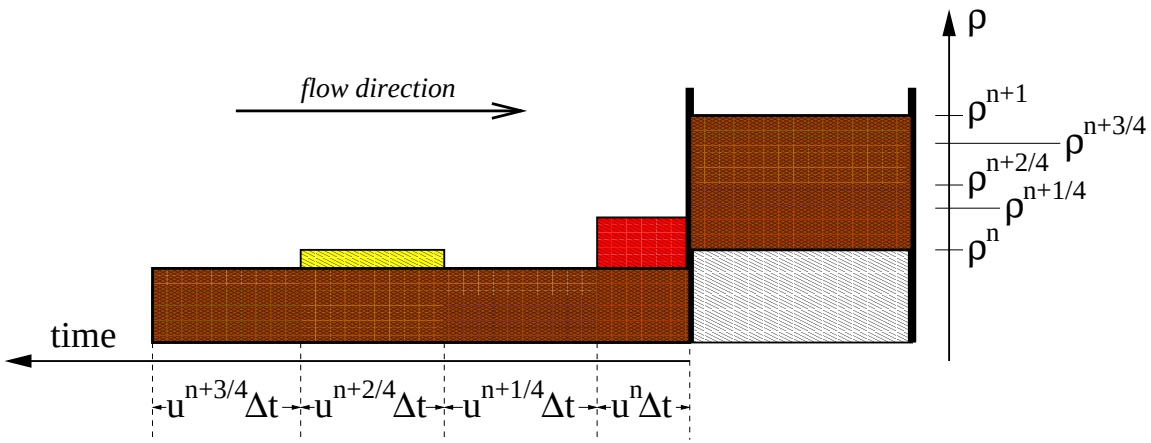

For efficiency, sub-cycle dynamics with respect to tracers:

- Solve continuity equation for air ρ_d together with momentum and thermodynamics equations.
- Repeat *ksplit* times
- Brown area = average flow of mass through cell face.
- Compute time-averaged value of m across brown area using flux-form scheme: $\overline{\overline{< m >}}$.
- Flux of tracer mass: $\overline{\overline{< m >}} \times \sum_{i=1}^{ksplit} {\rho_d}^{n+i/ksplit}$
- Yields 'free stream' preserving solution!

Vertical coordinate: hybrid sigma ($\sigma = p/p_s$)-pressure (p) coordinate

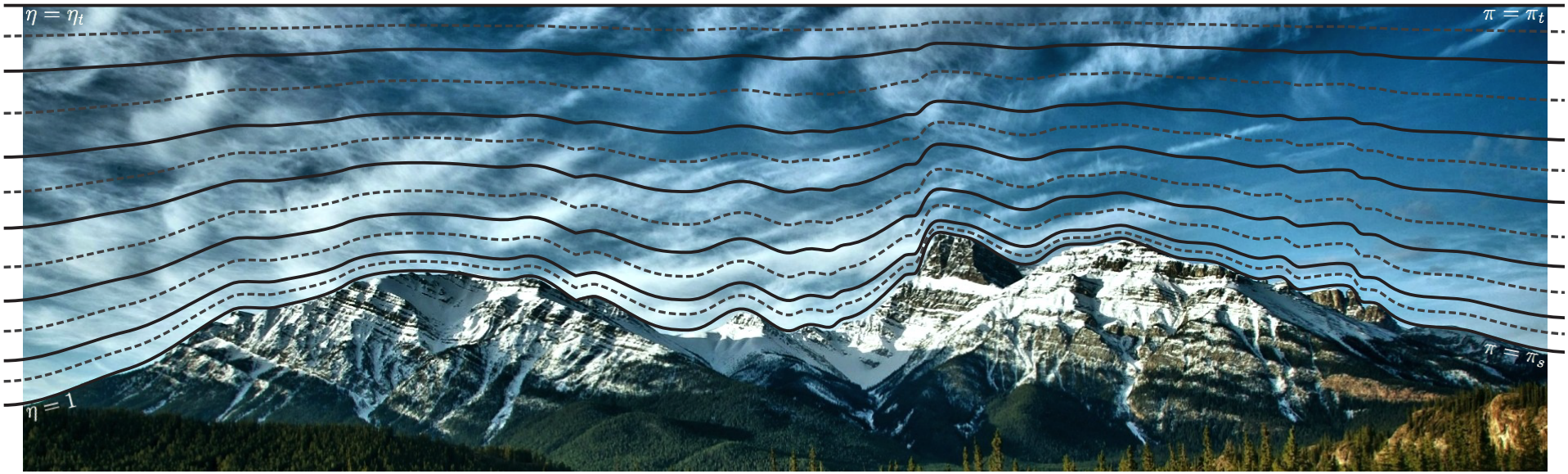

Figure courtesy of David Hall (CU Boulder).

Sigma layers at the bottom (following terrain) with isobaric (pressure) layers aloft.

Pressure at model level interfaces

$$p_{k+1/2} = A_{k+1/2}\, p_0 + B_{k+1/2}\, p_s,$$

where p_s is surface pressure, p_0 is the model top pressure, and $A_{k+1/2} (\in [0:1])$ and $B_{k+1/2} (\in [1:0])$ hybrid coefficients (in model code: *hyai* and *hybi*). Similarly for model level mid-points.

Note: vertical index is 1 at model top and *klev* at surface.

Why do we use terrain-following coordinates?

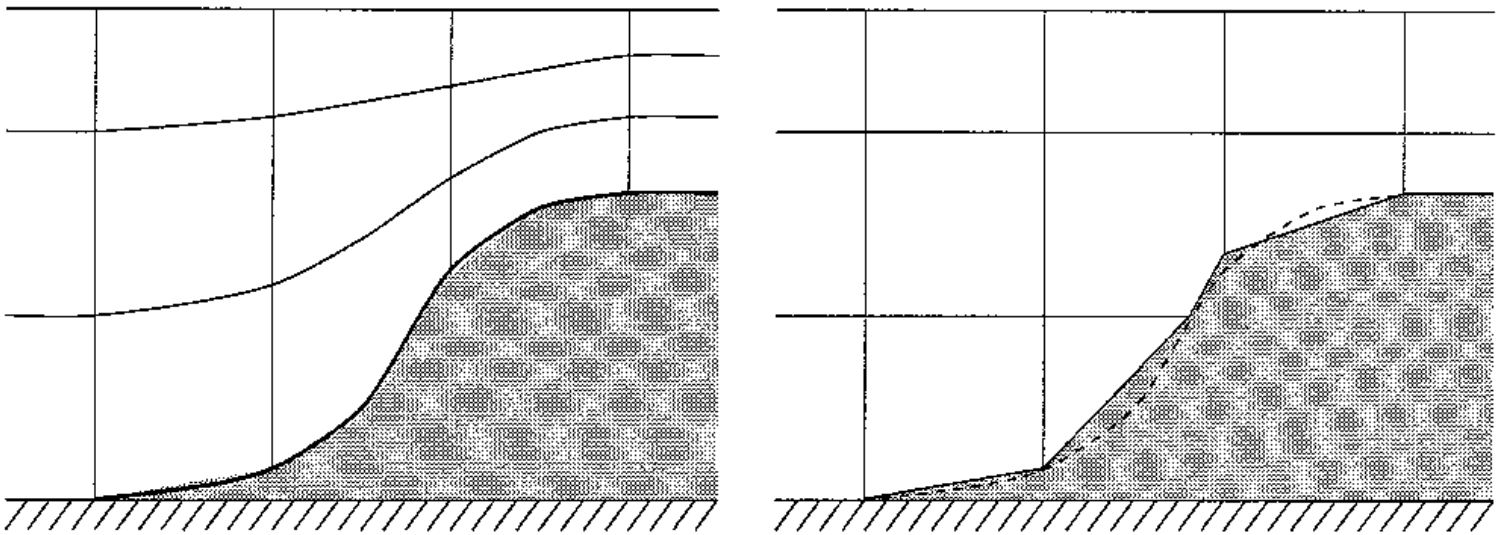

Figure: Representation of a smoothly varying bottom (dashed line) in (left) a terrain-following coordinate model, and (right) a height coordinate model with piecewise constant slopes (cut-cells, shaved-cells)

Figure is from Adcroft et al. (1997).

$\rightarrow$ The main reason is that the lower boundary condition is very simple when using terrain-following coordinates!

Aside: hybrid sigma ($\sigma = p/p_s$)-pressure (p) coordinate

While terrain-following coordinates simplify the bottom boundary condition, they may introduce errors:

- Pressure gradient force (PDF) errors: $\frac{1}{\rho_d}\nabla p_z = \frac{1}{\rho_d}\nabla_\eta p + \frac{1}{\rho_d}\frac{dp}{dz}\nabla_\eta z$, (Kasahara, 1974) where ρ_d is density, p pressure and z height.
- Errors in modeling flow along constant z-surfaces near the surface

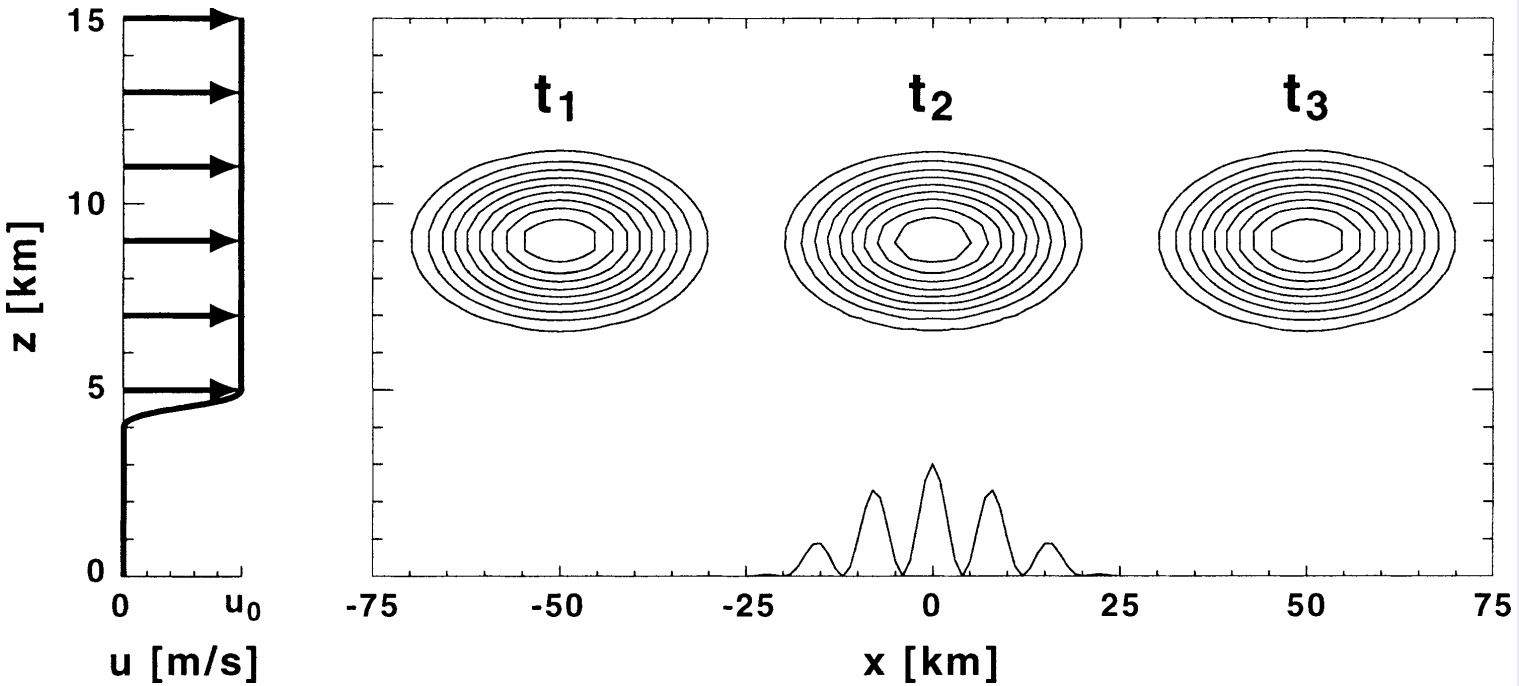

FIG. 4. Vertical cross section of the idealized two-dimensional advection test. The topography is located entirely within a stagnant pool of air, while there is a uniform horizontal velocity aloft. The analytical solution of the advected anomaly is shown at three instances.

Schär et al. (2002)

Aside: hybrid sigma ($\sigma = p/p_s$)-pressure (p) coordinate

While terrain-following coordinates simplify the bottom boundary condition, they may introduce errors:

- Pressure gradient force (PDF) errors: $\frac{1}{\rho_d}\nabla p_z = \frac{1}{\rho_d}\nabla_\eta p + \frac{1}{\rho_d}\frac{dp}{dz}\nabla_\eta z$, (Kasahara, 1974) where ρ_d is density, p pressure and z height.
- Errors in modeling flow along constant z-surfaces near the surface

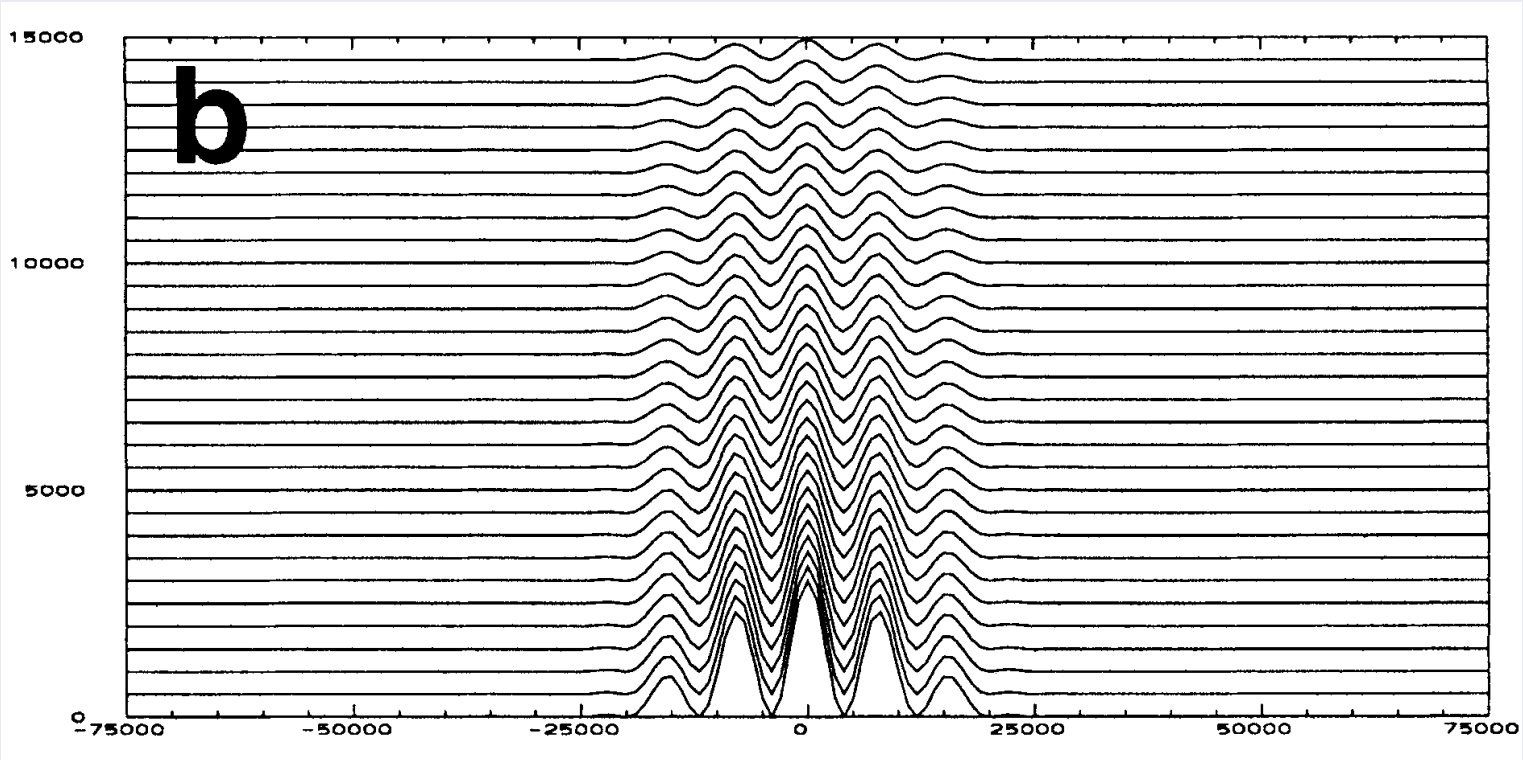

Schär et al. (2002)

Aside: hybrid sigma ($\sigma = p/p_s$)-pressure (p) coordinate

While terrain-following coordinates simplify the bottom boundary condition, they may introduce errors:

- Pressure gradient force (PDF) errors: $\frac{1}{\rho_d}\nabla p_z = \frac{1}{\rho_d}\nabla_\eta p + \frac{1}{\rho_d}\frac{dp}{dz}\nabla_\eta z$, (Kasahara, 1974) where ρ_d is density, p pressure and z height.
- Errors in modeling flow along constant z-surfaces near the surface

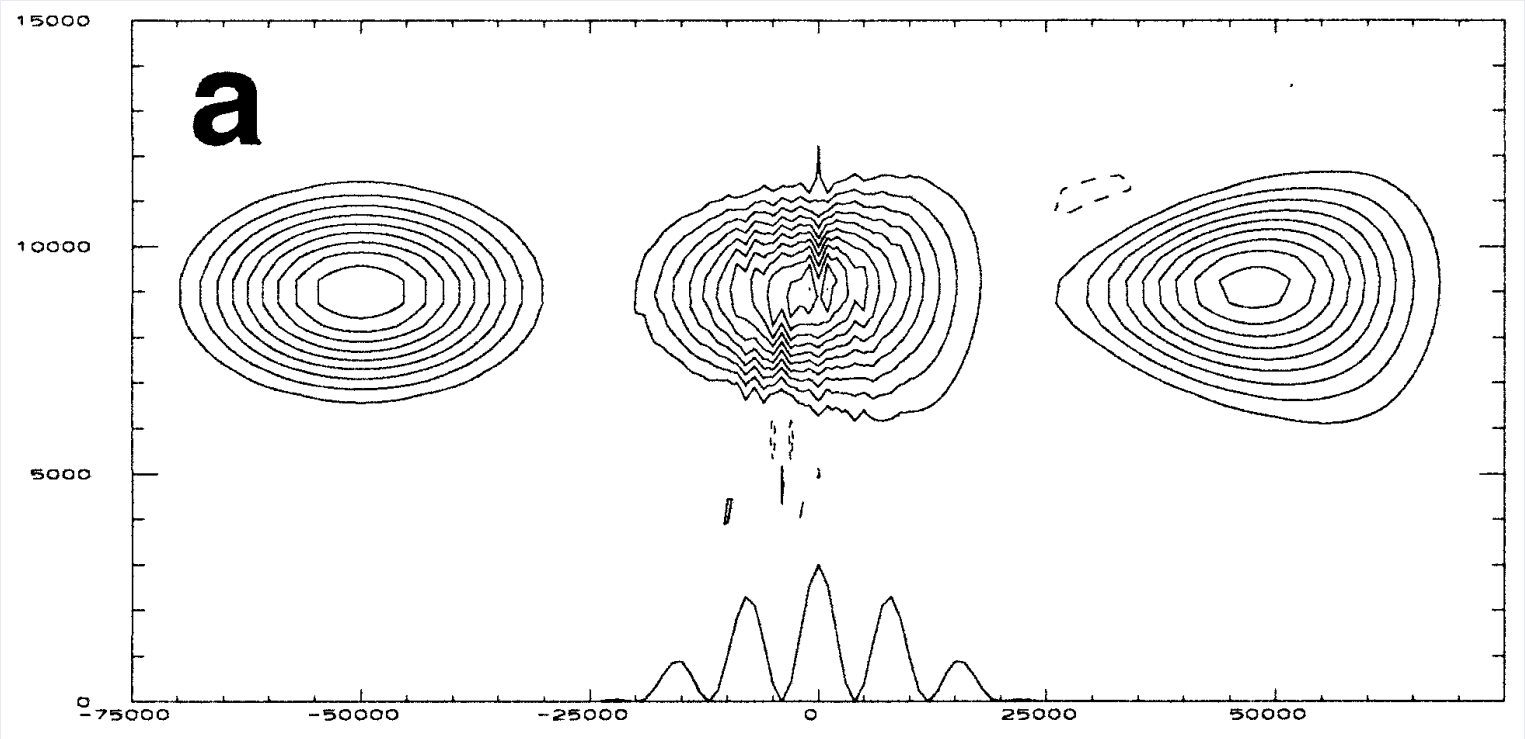

Schär et al. (2002)

Vertical coordinate

- Lagrangian ('floating') vertical coordinate ξ so that

$$\frac{d\xi}{dt} = 0,$$

  i.e. vertical surfaces are material surfaces (no flow across them).

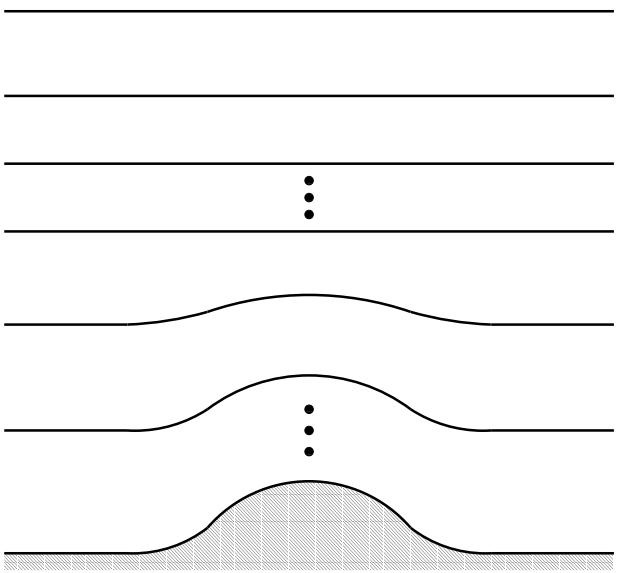

Figure shows 'usual' hybrid $\sigma - p$ vertical coordinate $\eta(p_s, p)$ (where p_s is surface pressure):

- $\eta(p_s, p)$ is a monotonic function of p.
- $\eta(p_s, p_s) = 1$
- $\eta(p_s, 0) = 0$
- $\eta(p_s, p_{top}) = \eta_{top}$.

Boundary conditions are:

- $\frac{d\eta(p_s,p_s)}{dt} = 0$
- $\frac{d\eta(p_s,p_{top})}{dt} = \omega(p_{top}) = 0$

  (ω is vertical velocity in pressure coordinates)

Vertical coordinate

- Lagrangian ('floating') vertical coordinate ξ so that

$$\frac{d\xi}{dt} = 0,$$

i.e. vertical surfaces are material surfaces (no flow across them).

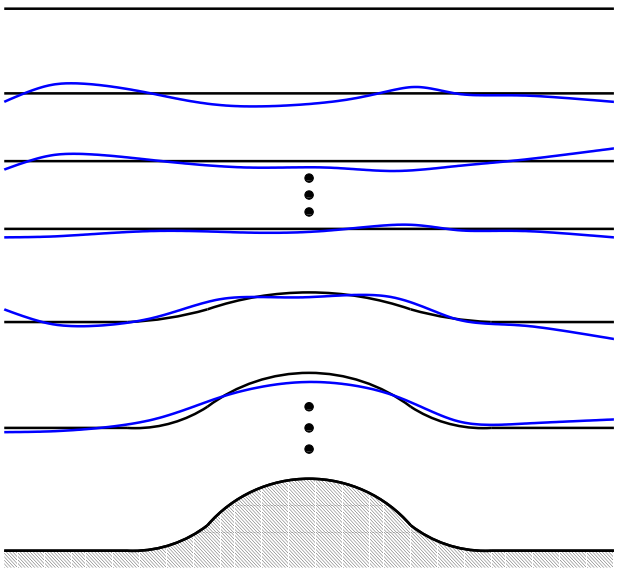

Figure:

- set $\xi = \eta$ at time t_{start} (black lines).
- for $t > t_{start}$ the vertical levels deform as they move with the flow (blue lines).
- to avoid excessive deformation of the vertical levels (non-uniform vertical resolution) the prognostic variables defined in the Lagrangian layers ξ are periodically remapped (= conservative interpolation) back to the Eulerian reference coordinates η (more on this later).

Why use floating Lagrangian vertical coordinates?
Vertical advection terms disappear (3D model becomes 'stacked shallow-water models'; only 2D numerical methods are needed)

The spectral-element method: discretization grid

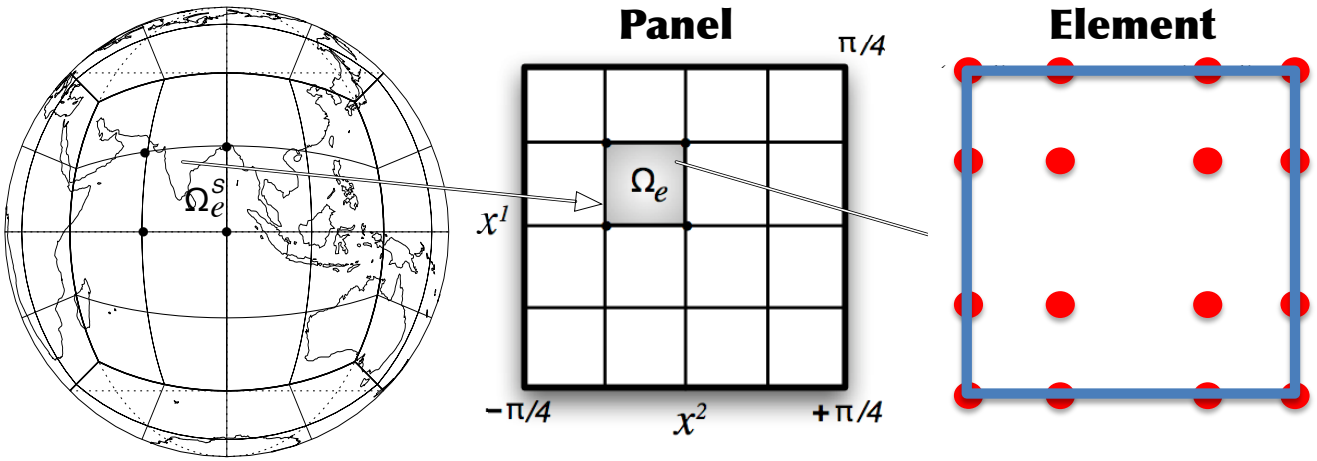

Physical Domain | Computational Domain | GLL Quadrature Grid

Nodal 1D polynomial basis functions

GLL=Gauss-Lobatto-Legendre

The spectral-element method: discretization grid

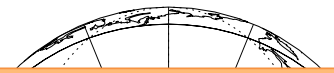

For any arbitrary variable f (e.g., T, u, v, p, ...) one can approximate f as a function of a tensor product of 1D basis functions on the 2D GLL grid:

$$f(x,y) = \sum_{i,j} f_{i,j} h_i(x_i) h_j(y_j),$$

where $f_{i,j}$ is grid point values of f.

Physical Domain | Computational Domain | GLL Quadrature Grid

Nodal 1D polynomial basis functions

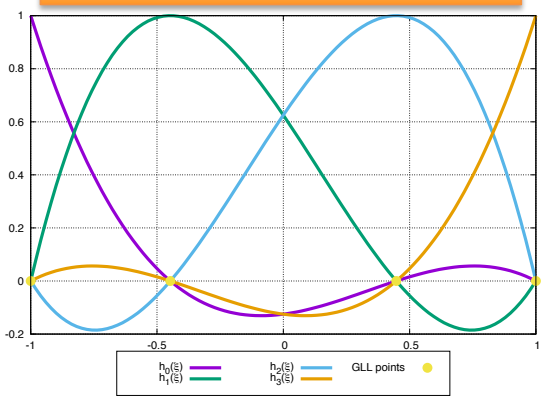

GLL=Gauss-Lobatto-Legendre

The spectral-element method

Spectral-Element Method (SEM)

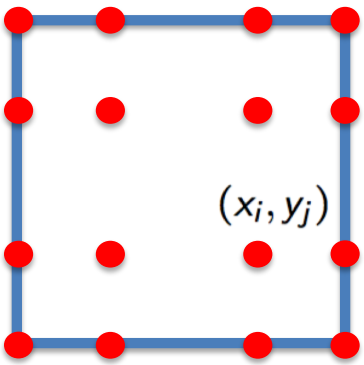

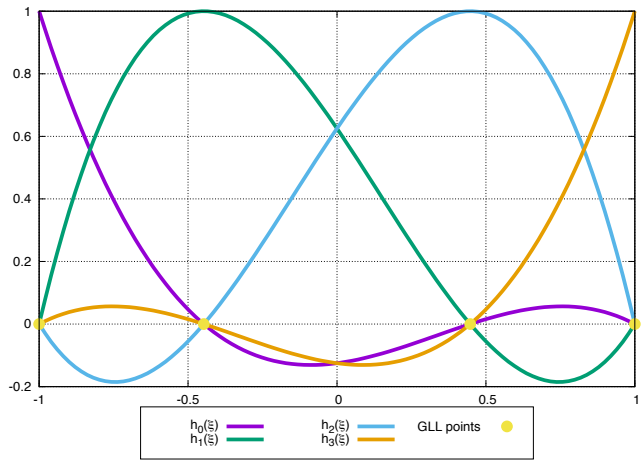

Continuity equation for Δp:

$$\frac{\partial \Delta p}{\partial t} = -\nabla \cdot \Delta p \vec{v} + \tau \nabla^4 \Delta p.$$

The spectral-element method

Spectral-Element Method (SEM)

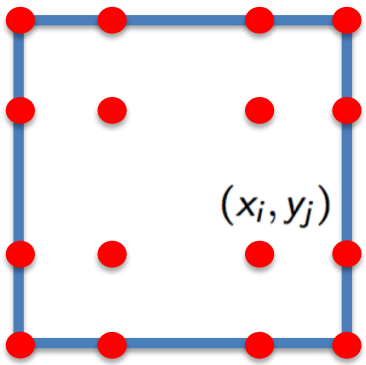

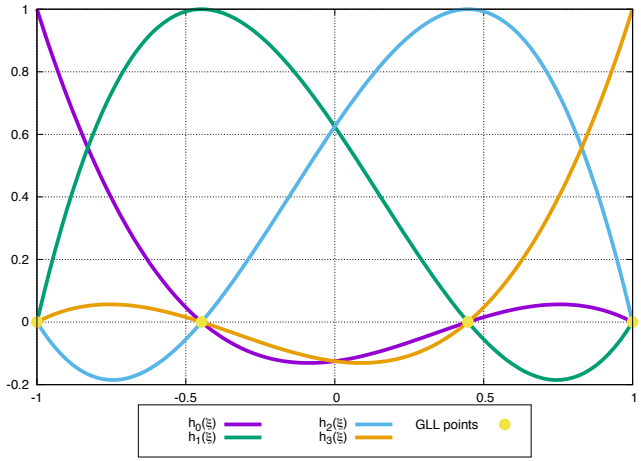

Continuity equation for Δp:

$$\left\langle h_k, \frac{\partial \Delta p}{\partial t} \right\rangle = \langle h_k, -\nabla \cdot \Delta p \vec{v} \rangle + \left\langle h_k, \tau \nabla^4 \Delta p \right\rangle,$$

where $\langle h_k, \cdot \rangle$ is inner product

$$\langle h_k, f \rangle = \sum_{i,j} w_{i,j} h_k(x_i, y_j) f(x_i, y_j) \sim \iint h_k f \, dA.$$

The spectral-element method

Spectral-Element Method (SEM)

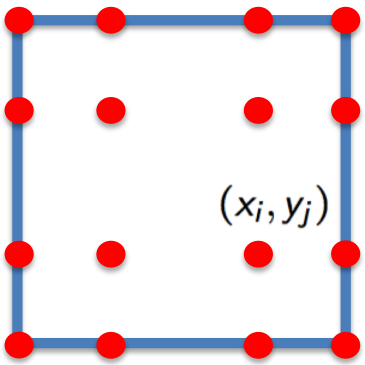

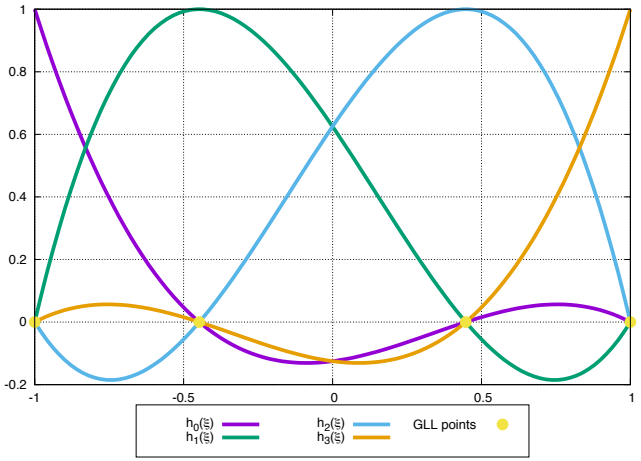

Continuity equation for Δp:

$$\left\langle h_k, \frac{\Delta p^* - \Delta p^n}{\Delta t} \right\rangle = \langle h_k, -\nabla \cdot \Delta p \vec{v} \rangle + \left\langle h_k, \tau \nabla^4 \Delta p \right\rangle .$$

Temporal discretization: multi-stage Runge-Kutta time-stepping

The spectral-element method

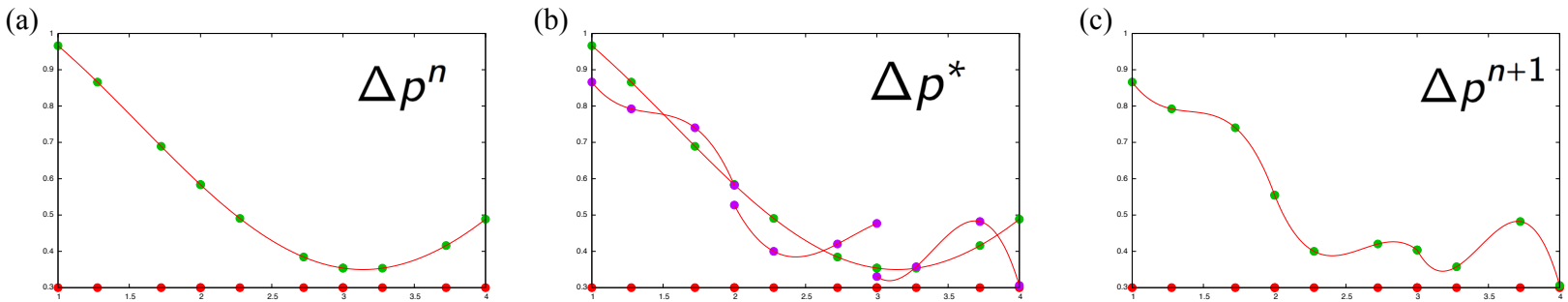

Continuity equation for Δp:

$$\left\langle h_k, \frac{\Delta p^* - \Delta p^n}{\Delta t} \right\rangle = \left\langle h_k, -\nabla \cdot \Delta p \vec{v} \right\rangle + \left\langle h_k, \tau \nabla^4 \Delta p \right\rangle .$$

Temporal discretization: multi-stage Runge-Kutta time-stepping

The spectral-element method

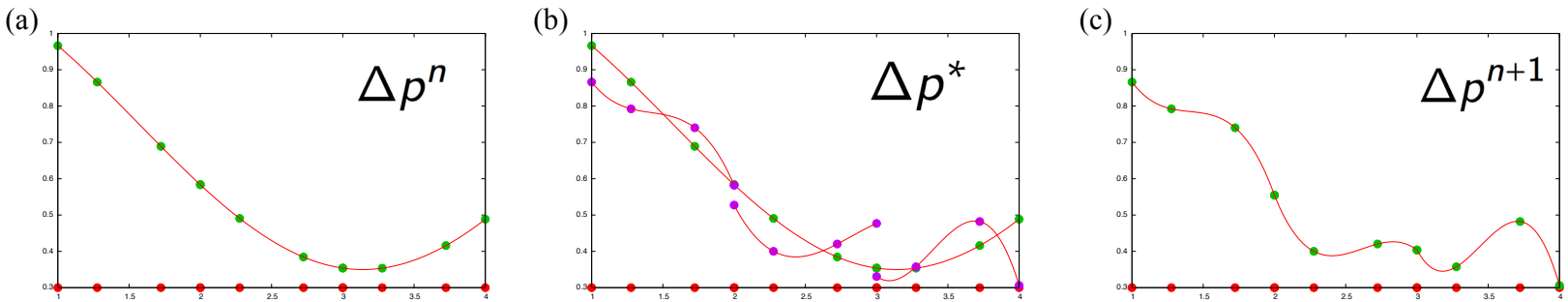

- Projection step

$$\Delta p^{n+1} = DSS\left(\Delta p^*\right)$$

where *DSS* refers to *Direct Stiffness Summation* (also referred to as assembly or inverse mass matrix step).

- Choice of GLL quadrature based inner product and nodal basis functions gives a diagonal mass matrix (Maday and Patera, 1987).

The spectral-element method

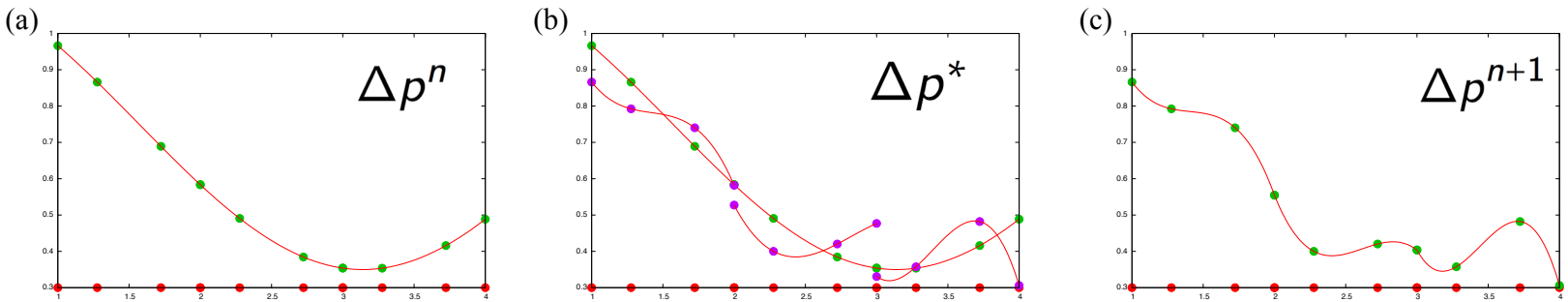

Continuity equation for Δp:

$$\left\langle h_k, \frac{\Delta p^{n+1} - \Delta p^n}{\Delta t} \right\rangle = \langle h_k, -\nabla \cdot \Delta p \vec{v} \rangle + \left\langle h_k, \tau \nabla^4 \Delta p \right\rangle + \langle h_k, D \rangle .$$

Temporal discretization: multi-stage Runge-Kutta time-stepping

CAM-SE-CSLAM (Herrington et al., 2018) - will be released with CESM2.1

CAM-SE has the option to run physics on a finite-volume grid that is coarser, same or finer resolution compared to the dynamics grid. This configuration uses inherently conservative CSLAM (Conservative Semi-LAgrangan Multi-tracer) transport scheme (Lauritzen et al., 2017).

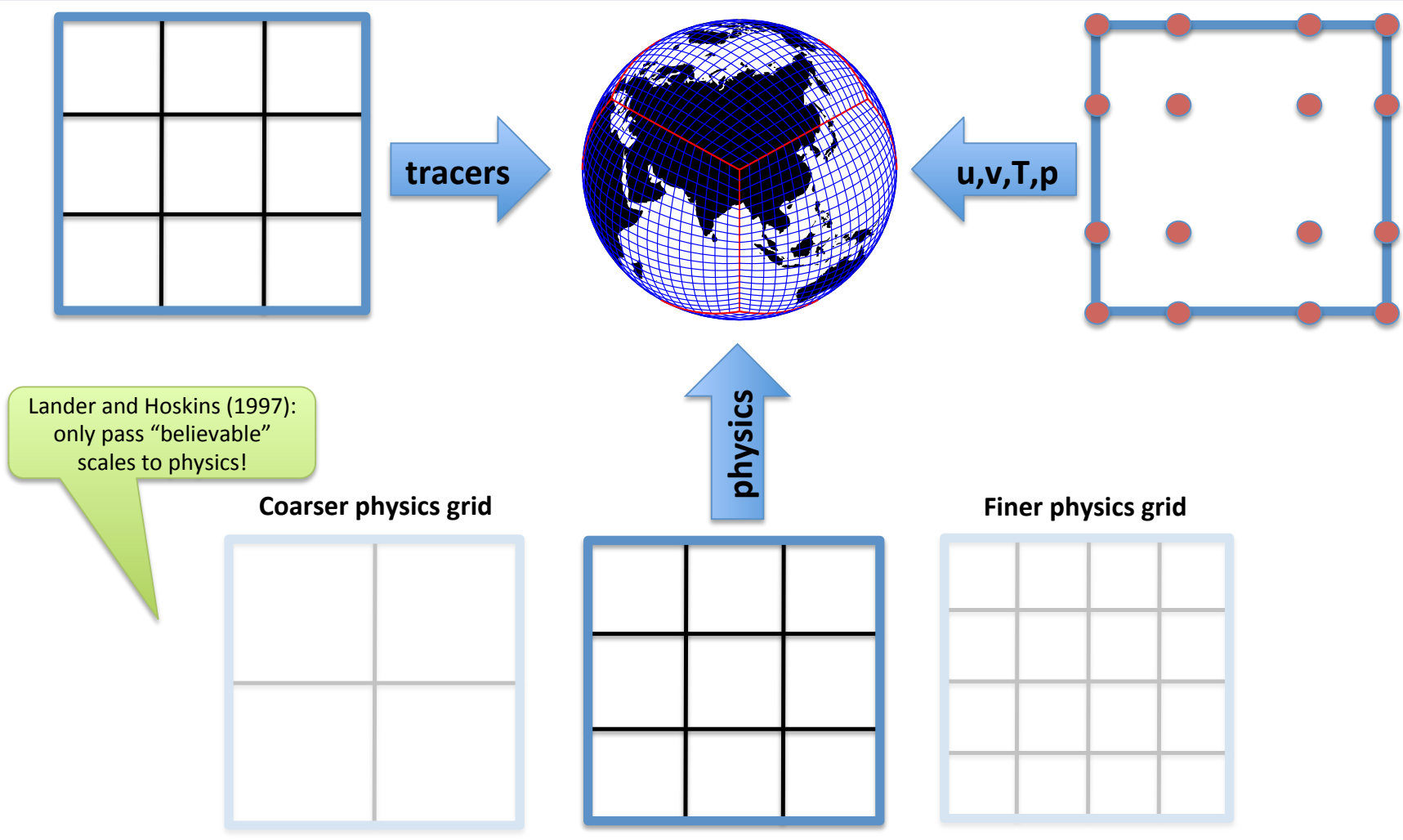

Summary

semi-Lagrangian form

Pros:

- allow for long time-steps: Δt limited by flow deformation (Lipschitz number and not by Courant number)
- less MPI communication; but more data to communicate
- geometric computations (weights) can be re-used for each additional tracer (multi-tracer efficiency)
- Lagrangian consistency

Cons:

- Lagrangian areas must span sphere without cracks/overlaps; and must find overlap areas (complex search algorithm)
- hard to extend to 3D (use Lagrangian vertical coordinate)

Eulerian (flux-form) form

Pros:

- fluxes can be computed in 'any' way (Lagrangian consistency not needed)
- many flux limiters in the literature (that said, FCT-type limiters need extra MPI communication)
- one can easily switch between time-stepping methods
- if flux computation is 'simple' then easy to extend to 3D

Cons:

- not stable for long time-steps (Courant number limited)
- more frequent MPI communications (each Runga-Kutta step; but less data to communicate compared to semi-Lagrangian schemes)

A standard test case suite for two-dimensional linear transport on the sphere: results from a collection of state-of-the-art schemes. - Lauritzen et al. (2014)

Questions?

References

Adcroft, A., Hill, C., and Marshall, J. (1997). Representation of topography by shaved cells in a height coordinate ocean model. *Mon. Wea. Rev.*, 125(9):2293–2315.

Barth, T. and Jespersen, D. (1989). The design and application of upwind schemes on unstructured meshes. *Proc. AIAA 27th Aerospace Sciences Meeting, Reno*.

Colella, P. and Woodward, P. R. (1984). The piecewise parabolic method (PPM) for gas-dynamical simulations. *J. Comput. Phys.*, 54:174–201.

Dennis, J. M., Edwards, J., Evans, K. J., Guba, O., Lauritzen, P. H., Mirin, A. A., St-Cyr, A., Taylor, M. A., and Worley, P. H. (2012). CAM-SE: A scalable spectral element dynamical core for the Community Atmosphere Model. *Int. J. High. Perform. C.*, 26(1):74–89.

Dukowicz, J. K. and Baumgardner, J. R. (2000). Incremental remapping as a transport/advection algorithm. *J. Comput. Phys.*, 160:318–335.

Durran, D. (2010). *Numerical Methods for Fluid Dynamics: With Applications to Geophysics*, volume 32 of *Texts in Applied Mathematics*. Springer, 2 edition. 516 p.

Godunov, S. K. (1959). A difference scheme for numerical computation of discontinuous solutions of equations in fluid dynamics. *Math. Sb.*, 47:271. Also: Cornell Aero. Lab. translation.

Harris, L. M., Lauritzen, P. H., and Mittal, R. (2010). A flux-form version of the conservative semi-Lagrangian multi-tracer transport scheme (CSLAM) on the cubed sphere grid. *J. Comput. Phys.*, 230(4):1215–1237.

Herrington, A. R., Lauritzen, P. H., Taylor, M. A., Goldhaber, S., Eaton, B. E., Reed, K. A., and Ullrich, P. A. (2018). Physics-dynamics coupling with element-based high-order Galerkin methods: quasi equal-area physics grid. *Mon. Wea. Rev.* revising.

Kasahara, A. (1974). Various vertical coordinate systems used for numerical weather prediction. *Mon. Wea. Rev.*, 102(7):509–522.

Lauritzen, P. H., Andronova, N., Bosler, P. A., Calhoun, D., Enomoto, T., Dong, L., Dubey, S., Guba, O., Hansen, A., Jablonowski, C., Juang, H.-M., Kaas, E., Kent, J., ller, R. M., Penner, J., Prather, M., Reinert, D., Skamarock, W., rensen, B. S., Taylor, M., Ullrich, P., and III, J. W. (2014). A standard test case suite for two-dimensional linear transport on the sphere: results from a collection of state-of-the-art schemes. *Geosci. Model Dev.*, 7:105–145.

Lauritzen, P. H., Erath, C., and Mittal, R. (2011a). On simplifying 'incremental remap'-type transport schemes. *J. Comput. Phys.*, 230:7957–7963.

Lauritzen, P. H., Kaas, E., Machenhauer, B., and Lindberg, K. (2008). A mass-conservative version of the semi-implicit semi-Lagrangian HIRLAM. *Q.J.R. Meteorol. Soc.*, 134.

Lauritzen, P. H., Nair, R., Herrington, A., Callaghan, P., Goldhaber, S., Dennis, J., Bacmeister, J. T., Eaton, B., Zarzycki, C., Taylor, M. A., Gettelman, A., Neale, R., Dobbins, B., Reed, K., and Dubos, T. (2018). NCAR CESM2.0 release of CAM-SE: A reformulation of the spectral-element dynamical core in dry-mass vertical coordinates with comprehensive treatment of condensates and energy. *J. Adv. Model. Earth Syst.*

Lauritzen, P. H., Nair, R. D., and Ullrich, P. A. (2010). A conservative semi-Lagrangian multi-tracer transport scheme (CSLAM) on the cubed-sphere grid. *J. Comput. Phys.*, 229:1401–1424.

Lauritzen, P. H., Taylor, M. A., Overfelt, J., Ullrich, P. A., Nair, R. D., Goldhaber, S., and Kelly, R. (2017). CAM-SE-CSLAM: Consistent coupling of a conservative semi-lagrangian finite-volume method with spectral element dynamics. *Mon. Wea. Rev.*, 145(3):833–855.

Lauritzen, P. H., Ullrich, P. A., and Nair, R. D. (2011b). Atmospheric transport schemes: desirable properties and a semi-Lagrangian view on finite-volume discretizations, in: P.H. Lauritzen, R.D. Nair, C. Jablonowski, M. Taylor (Eds.), Numerical techniques for global atmospheric models. *Lecture Notes in Computational Science and Engineering, Springer, 2011*, 80.

Lin, S. J. and Rood, R. B. (1996). Multidimensional flux-form semi-Lagrangian transport schemes. *Mon. Wea. Rev.*, 124:2046–2070.

Liu, X. D., Osher, S., and Chan, T. (1994). Weighted essentially non-oscillatory schemes. *J. Comput. Phys.*, 115:200–212.

Machenhauer, B., Kaas, E., and Lauritzen, P. H. (2009). Finite volume methods in meteorology, in: R. Temam, J. Tribbia, P. Ciarlet (Eds.), Computational methods for the atmosphere and the oceans. *Handbook of Numerical Analysis*, 14. Elsevier, 2009, pp.3-120.

Margolin, L. G. and Shashkov, M. (2003). Second-order sign-preserving conservative interpolation (remapping) on general grids. *J. Comput. Phys.*, 184:266–298.

Miura, H. (2007). An upwind-biased conservative advection scheme for spherical hexagonal-pentagonal grids. *Mon. Wea. Rev.*, 135:4038–4044.

Nair, R. D. and Machenhauer, B. (2002). The mass-conservative cell-integrated semi-Lagrangian advection scheme on the sphere. *Mon. Wea. Rev.*, 130(3):649–667.

Nair, R. D., Scroggs, J. S., and Semazzi, F. H. M. (2002). Efficient conservative global transport schemes for climate and atmospheric chemistry models. *Mon. Wea. Rev.*, 130(8):2059–2073.

Rančić, M. (1992). Semi-Lagrangian piecewise biparabolic scheme for two-dimensional horizontal advection of a passive scalar. *Mon. Wea. Rev.*, 120:1394–1405.

Schär, C., Leuenberger, D., Fuhrer, O., Lüthi, D., and Girard, C. (2002). A new terrain-following vertical coordinate formulation for atmospheric prediction models. *Mon. Wea. Rev.*, 130(10):2459–2480.

Skamarock, W. C., Klemp, J. B., Duda, M. G., Fowler, L., Park, S.-H., and Ringler, T. D. (2012). A multi-scale nonhydrostatic atmospheric model using centroidal Voronoi tesselations and C-grid staggering. *Mon. Wea. Rev.*, 240:3090–3105.

Skamarock, W. C. and Menchaca, M. (2010). Conservative transport schemes for spherical geodesic grids: High-order reconstructions for forward-in-time schemes. *Mon. Wea. Rev.*, 138:4497–4508.

Trenberth, K. E. and Smith, L. (2005). The mass of the atmosphere: A constraint on global analyses. *J. Climate*, 18:864–875.

Ullrich, P. A., Lauritzen, P. H., and Jablonowski, C. (2013). Some considerations for high-order 'incremental remap'-based transport schemes: edges, reconstructions and area integration. *Int. J. Numer. Meth. Fluids*, 71:1131–1151.

Wong, M., Skamarock, W. C., Lauritzen, P. H., and Stull, R. B. (2013). A cell-integrated semi-implicit semi-Lagrangian shallow-water model (CSLAM-SW) with consistent treatment of inherently-conservative mass and scalar mass transport. *Mon. Wea. Rev.*, 141:2545–2560.

Zalesak, S. T. (1979). Fully multidimensional flux-corrected transport algorithms for fluids. *J. Comput. Phys.*, 31:335–362.

Zerroukat, M., Wood, N., and Staniforth, A. (2002). SLICE: A semi-Lagrangian inherently conserving and efficient scheme for transport problems. *Q. J. R. Meteorol. Soc.*, 128:2801–2820.

Zerroukat, M., Wood, N., and Staniforth, A. (2005). A monotonic and positive-definite filter for a semi-Lagrangian inherently conserving and efficient (SLICE) scheme. *Q. J. R. Meteorol. Soc.*, 131(611):2923–2936.